4500

Three-Dimensional Simulation of Steamflooding

K. H. COATS
MEMBER SPE-AIME
W. D. GEORGE
CHIEH CHU
MEMBER SPE-AIME
B. E. MARCUM
MEMBER SPE-AIME

INTERCOMP RESOURCE DEVELOPMENT AND ENGINEERING, INC.
HOUSTON, TEX.
GETTY OIL CO.
HOUSTON, TEX.
GETTY OIL CO.
LOS ANGELES, CALIF.

ABSTRACT

This paper describes a three-dimensional model for numerical simulation of steam injection processes. The model describes three-phase flow of water, oil, and steam and heat flow in the reservoir and overburden. The method of solution simultaneously solves for the mass and energy balances and eliminates the need for iterating on the mass transfer (condensation) term.

Laboratory data are reported for steamfloods of 5,780-cp oil in a 1/4 five-spot sand pack exhibiting three-dimensional flow effects. These experiments provide additional data for checking accuracy and assumptions in numerical models.

Comparisons of model results with several sets of experimental data indicate a need to account for effects of temperature on relative permeability. Calculated areal conformance of a steamflood in a confined five-spot depends strongly upon the alignment of the x-y grid axes relative to the diagonal joining injection and production wells. It has not been determined which, if either, of the two grid types yields the correct areal conformance.

Model calculations indicate that steamflood pressure level strongly affects oil recovery. Calculated oil recovery increases with decreasing pressure level. An example application illustrates the ability of the model formulation to efficiently simulate the single-well, cyclic steam stimulation problem.

INTRODUCTION

The literature includes many papers treating various aspects of oil recovery by steamflooding, hot waterflooding, and steam stimulation. The papers present laboratory experimental data, field performance results, models for calculating fluid and heat flow, and experimental data regarding effects of temperature on relative permeability. The ultimate goal of all this work is a reliable engineering analysis to estimate oil recovery for a given mode of operation and to determine alternative operating conditions to maximize oil recovery.

Toward that end, our study proposed to develop and validate an efficient, three-dimensional numerical model for simulating steamflooding, hot waterflooding, and steam stimulation. Laboratory steamflood experiments were conducted to provide additional data for validation. Desired model specifications included three-dimensional capability and greater efficiency than reported for previous models. Omitted from the specifications were temperature-dependent relative permeability and steam distillation effects.

This paper describes the main features of the three-dimensional, steamflood model developed. Those features include a new method of solution that includes implicit water transmissibilities, that simultaneously solves for mass and energy balances, and that eliminates the need for iteration on the condensation term. Laboratory data are reported for steamfloods in a 1/4 five-spot model exhibiting three-dimensional flow effects. Numerical model applications described include comparisons with experimental data, a representative field-scale steamflood, and a cyclic steam stimulation example.

REVIEW OF PREVIOUS WORK

Early efforts in mathematical modeling of thermal methods[1-5] concentrated on simulation of the heat flow and heat loss. Gottfried,[6] in his analysis of in-situ combustion, initiated a series of models that solve fluid mass balances along with the energy balance. Davidson *et al.*[7] presented an analysis for well performance during cyclic steam injection. Spillette and Nielsen[8] treated hot waterflooding in two dimensions. Shutler described three-phase models for linear[9] and two-dimensional[10] steamflooding, and Abdalla and Coats[11] treated a two-dimensional steamflood model using the IMPES method of solution. Most recently, Shutler and Boberg[12] presented an approximate analytical

Original manuscript received in Society of Petroleum Engineers office Sept. 4, 1974. Revised manuscript received Aug. 7, 1974. Paper (SPE 4500) was first presented at the SPE-AIME 48th Annual Fall Meeting, held in Las Vegas, Nev., Sept. 30-Oct. 3, 1973.

[1] References listed at end of paper.

This paper will be printed in *Transactions* volume 257, which will cover 1974.

method for calculating linear steamflood performance.

Willman *et al.*[3] reported oil recovery curves and temperature distributions obtained during laboratory steamfloods and hot waterfloods of viscous oils in linear cores. Crichlow[13] presented temperature distributions obtained during laboratory displacements of cold water by hot water and by steam in a linear sand pack. Baker[14,15] gave temperature and water saturation distributions resulting from cold water displacement by steam in a disk-shaped sand pack. Abdalla and Coats[11] reported oil recovery curves for linear-core steamfloods, and Shutler[10] gave oil recovery curves for continuous and bank injection of steam in a 1/8 five-spot laboratory model.

Several authors[16-19] have described laboratory studies of the effect of temperature on relative permeabilities. In the most recent of those studies, Weinbrandt and Ramey[19] concluded that a moderate 100°F temperature rise in a water-oil system can nearly double irreducible water saturation and reduce residual oil saturation by more than half. de Haan and van Lookeren[20] reported that in their steam stimulation field operation, only about one-fourth of injected steam was recovered as water production. The possible connection between this observation and the above mentioned effect of temperature on irreducible water is obvious.

MODEL DESCRIPTION

The model consists of five equations expressing conservation of energy; conservation of mass for water, steam, and oil; and steam-water equilibrium. In finite-difference form, these equations are

Water

$$-q_c + \frac{V}{\Delta t}\delta(\phi b_w S_w) = \Delta(T_w(\Delta p_w - \gamma_w \Delta Z)) - q_w \quad \ldots\ldots\ldots\ldots\ldots\ldots\ldots\ldots (1)$$

Steam

$$q_c + \frac{V}{\Delta t}\delta(\phi b_g S_g) = \Delta(T_g(\Delta p_g - \gamma_g \Delta Z)) - q_g \quad \ldots\ldots\ldots\ldots\ldots\ldots\ldots\ldots (2)$$

Oil

$$\frac{V}{\Delta t}\delta(\phi b_o S_o) = \Delta(T_o(\Delta p_o - \gamma_o \Delta Z)) - q_o, \quad \ldots\ldots\ldots\ldots\ldots\ldots\ldots\ldots (3)$$

Energy

$$\frac{V}{\Delta t}\delta\left[\phi(b_w S_w U_w + b_o S_o U_o + b_g S_g U_g) + (1-\phi)(\rho C_p)_R T\right] = \Delta(T_H \Delta p) + \Delta(T_c \Delta T) - q_L - q_H \quad \ldots\ldots (4)$$

Equilibrium

$$T = T_s(p) \quad \ldots\ldots\ldots\ldots\ldots\ldots\ldots\ldots (5)$$

The term $\Delta(T_H \Delta p)$ in Eq. 4 denotes the net enthalpy flow into the grid block due to interblock water, steam, and oil mass flow rates. The term q_H is enthalpy production due to fluid production, and q_L is rate of heat loss to strata above and below the reservoir formation. Detailed definitions of these and other terms are given in the Nomenclature.

A verbal statement of the energy equation is basically "enthalpy in − enthalpy out = change or gain in internal energy of system," where the open system is the grid block volume, V, and its contained rock and fluids. This energy balance is rigorous except for kinetic energy and potential energy terms, which have been neglected.

The transmissibilities for flow between any two blocks require some effective or average interblock values of relative permeability, formation volume factor, viscosity, and in the case of the energy equation, enthalpy. Relative permeability and enthalpy are weighted 100 percent upstream. Formation volume factor and viscosity are, in most cases, evaluated as the arithmetic average of the values in the two blocks.

Tables of relative permeability and capillary pressure vs saturation are read into the simulator for two-phase water-oil and gas-oil systems. Three-phase relative permeabilities are then calculated using Stone's method.[21] Linear interpolation is used between adjacent entries in the tables. Viscosities are entered into the simulator as tabular functions of temperature. Interpolation between adjacent entries is performed assuming linearity of log μ vs log T between the entries.

The model is based on an assumption of negligible steam distillation effects. That is, the oil is assumed to liberate (as "gas") an insignificant portion of its original mass over the pressure and temperature ranges occurring during contact with injected steam. In actuality, the oil will exchange light ends with the steam-hydrocarbon gas phase, at any pressure and temperature where a gas phase exists, so as to establish equilibrium. Rigorous treatment of this equilibrium is rendered difficult by the dependence of the equilibrium compositions upon K-values, which are in turn dependent upon pressure, temperature, and composition.

METHOD OF SOLUTION

Our method of solution differs in three major respects from the methods reported by Shutler[9] and Abdalla.[11] First, we eliminate the condensation (mass transfer) term by combining the water and steam balance equations. The condensation rate is thus implicitly represented within a set of four equations. We found that considerable computational difficulties can arise when this rate is left as a term in the equations requiring iteration. Second, we solve the mass and energy balances simultane-

ously as opposed to using a staged calculation where pressures and saturations are calculated from mass balances and temperature is then calculated from the energy balance. Third, we treat water transmissibilities implicitly, thus reducing instabilities arising from explicit transmissibility calculations.

Oil and water formation volume factors are represented as functions of pressure and temperature as

$$b_w = b_{wi}\left[1+c_w(p-p_i)-C_{Tw}(T-T_i)\right], \quad (6)$$

$$b_o = b_{oi}\left[1+c_o(p-p_i)-C_{To}(T-T_i)\right], \quad (7)$$

where C_T denotes coefficient of thermal expansion and b_{wi}, b_{oi} are water and oil formation volume factors at p_i, T_i. Porosity is treated as a function of pressure as

$$\phi = \phi_i(1+c_r(p-p_i)). \quad (8)$$

Internal energies of water and oil are represented as

$$U_w = U_{wi}+C_{pw}(T-T_i), \quad (9)$$

$$U_o = C_{po}(T-T_i). \quad (10)$$

Steam formation volume factor, b_g, and internal energy, U_g, are taken directly from the steam tables. All enthalpies are computed as $U + p/\rho$, where ρ is density.

Early in the model development, individual phase pressures were used to determine corresponding phase properties. Later comparisons showed insignificant error due to evaluating all phase properties from a single pressure. Pressure p in equations presented here denotes oil-phase pressure.

The terms in the left-hand side of Eqs. 1 through 4 are simple time differences of type $\delta\chi$. The identity

$$\delta\chi \equiv \chi_{n+1}-\chi_n, \quad (11)$$

where n denotes time level, must be carefully preserved in expansions. For example, the expansion

$$\delta(\phi b_w S_w U_w) = U_{wn+1}\delta(\phi b_w S_w)+(\phi b_w S_w)_n \delta U_w$$

$$= U_{wn+1}\left[(\phi b_w)_{n+1}\delta S_w + S_{wn}(\phi_{n+1}(b_{wp}\delta p+b_{wT}\delta T) + b_{wn}\phi_i c_r \delta p)\right] + (\phi b_w S_w)_n C_{pw}\delta T \quad (12)$$

is an expansion of $\delta(\phi b_w S_w U_w)$ in terms of δp, δT, δS_w, which is consistent or exact in the sense that it satisfies the identity

$$\delta(\phi b_w S_w U_w) \equiv (\phi b_w S_w U_w)_{n+1} - (\phi b_w S_w U_w)_n. \quad (13)$$

All terms on the left-hand side of Eqs. 1 through 5 can be expanded in the manner indicated in terms of the four unknowns δS_g, δS_w, δT and δp. The term δS_o arises but can be replaced by $-(\delta S_w + \delta S_g)$.

Phase pressures in the flow terms of Eqs. 1 through 5 are expressed at time level $n + 1$ except that capillary pressures are held explicit at time level n. Transmissibilities T_w, T_H, etc., and phase densities are explicitly represented in terms of relative permeabilities, enthalpy, pressure, and temperature at time level n. The conduction term is explicit in terms of temperature T at time level n. The heat-loss term is implicitly represented as $q_{Ln} + a\delta T$ as described in the Appendix.

If steam is present, then the equilibrium equation (Eq. 5) can be expanded as

$$T_{n+1} = T_s(p_{n+1}) = T_{sn} + T_{sp}\delta p, \quad (14)$$

where T_{sn} is $T_s(p_n)$ and T_{sp} is the chord slope,

$$T_{sp} = \frac{T_{sn+1}-T_{sn}}{P_{n+1}-p_n}. \quad (15)$$

T_{sp} must be determined by iteration during the time step using the nonlinear $T_s(p)$ function as given in the steam tables.[30] Subtracting T_n from both sides of Eq. 14 gives the following simple relation between δT and δp.

$$\delta T = T_{sn}-T_n+T_{sp}\delta p. \quad (16)$$

If no steam is present at time t_{n+1}, then Eq. 5 is simply

$$\delta S_g = -S_{gn}. \quad (17)$$

Addition of Eqs. 1 and 2 cancels the condensation term q_c and results in the following set of four equations:

$$C_{11}\delta S_g+C_{12}\delta S_w+C_{13}\delta T+C_{14}\delta p = \Delta((T_w+T_g)\Delta\delta p)+R_1, \quad (18)$$

$$C_{21}\delta S_g+C_{22}\delta S_w+C_{23}\delta T+C_{24}\delta p = \Delta(T_o\Delta\delta p)+R_2, \quad (19)$$

$$C_{31}\delta S_g+C_{32}\delta S_w+C_{33}\delta T+C_{34}\delta p = \Delta(T_H\Delta\delta p)+R_3 \quad \ldots\ldots\ldots\ldots (20)$$

$$C_{41}\delta S_g + C_{43}\delta T+C_{44}\delta p = R_4 . \quad (21)$$

Eq. 21 represents either Eq. 16 or Eq. 17, depending upon whether steam is present at the end of the time step. A partial list of definitions of coefficients C_{ij} and residuals R_i is as follows:

$$C_{11} = \frac{V}{\Delta t}(\phi b_g)_{n+1}$$

$$C_{14} = \frac{V}{\Delta t}[S_{wn}(\phi_{n+1}b_{wp}+\phi_i c_r b_{wn}) + S_{gn}(\phi_{n+1}b_{gp}+\phi_i c_r b_{gn})]$$

$$= C_{14w}+C_{14g}$$

$$C_{34} = U_{wn+1}C_{14w}+U_{gn+1}C_{14g}+U_{on+1}C_{24}$$

$$R_1 = \Delta(T_w(\Delta p_{wn}-\gamma_w\Delta Z)) + \Delta(T_g(\Delta p_{gn}-\gamma_g\Delta Z)) - q_{wn}-q_{gn}$$

Eqs. 18 through 21 are four equations in the four unknowns, δS_g, δS_w, δT and δp. They can be expressed in matrix form as

$$C\,\underline{P} = I\,\underline{Y} + \underline{R} , \quad \ldots\ldots\ldots (22)$$

where C is the 4×4 matrix $[C_{i,j}]$, I is the identity matrix,

$$\underline{P} = \begin{bmatrix} \delta S_g \\ \delta S_w \\ \delta T \\ \delta p \end{bmatrix} \quad \underline{Y} = \begin{bmatrix} y_1 \\ y_2 \\ y_3 \\ 0 \end{bmatrix} \quad \underline{R} = \begin{bmatrix} R_1 \\ R_2 \\ R_3 \\ R_4 \end{bmatrix}$$

$$\ldots\ldots\ldots\ldots\ldots\ldots (23)$$

and $y_1 = \Lambda[(T_w + T_g)\Lambda\delta p]$, $y_2 = \Lambda(T_o\,\Lambda\delta p)$ and $y_3 = \Lambda(T_H\Delta\delta p)$. Gaussian elimination reduces Eq. 22 to the form

$$\begin{bmatrix} 1 & C'_{12} & C'_{13} & C'_{14} \\ 0 & 1 & C'_{23} & C'_{24} \\ 0 & 0 & 1 & C'_{34} \\ 0 & 0 & 0 & C'_{44} \end{bmatrix} \begin{bmatrix} \delta S_g \\ \delta S_w \\ \delta T \\ \delta p \end{bmatrix} =$$

$$\begin{bmatrix} B_{11} & 0 & 0 & 0 \\ B_{21} & B_{22} & 0 & 0 \\ B_{31} & B_{32} & B_{33} & 0 \\ B_{41} & B_{42} & B_{43} & 1 \end{bmatrix} \begin{bmatrix} Y_1 \\ Y_2 \\ Y_3 \\ 0 \end{bmatrix} + \begin{bmatrix} R'_1 \\ R'_2 \\ R'_3 \\ R'_4 \end{bmatrix}$$

$$\ldots\ldots\ldots\ldots\ldots\ldots (24)$$

The last of these four equations is

$$C'_{44}\delta p = B_{41}\Delta((T_w+T_g)\Delta\delta p) + B_{42}\Delta(T_o\Delta\delta p) + B_{43}\Delta(T_H\Delta\delta p)+R'_4 , \quad \ldots (25)$$

which is a parabolic difference equation in pressure of the type commonly encountered in reservoir simulation problems. Eq. 25 can be solved by an iterative method such as ADI, SIP, and LSOR, or by direct solution.

We have selected the reduced band-width direct solution methods described by Price and Coats.[22] One reason for this selection is that for most reservoir problems, less computer time is required, compared with any iterative method. A second, more important reason is that a physically real negative transmissibility can occur in the pressure equation, and iterative methods generally require positive transmissibility to achieve convergence.

After Eq. 25 is solved for δp, the third, second, and first of the four Eqs. 24 can be solved for δT, δS_w and δS_g, respectively. One iteration consists of solving Eq. 25 for δp and then calculating δT, Temperature- and pressure-dependent coefficients C_{ij} are then updated and Eq. 25 is again solved for δp. This constitutes a second iteration. The iterations are continued until the following tolerances are met:

$$\max_{\text{over grid}} \left|\delta p^{\ell+1}-\delta p^{\ell}\right| \le \text{TOLP} ,$$

$$\max_{\text{over grid}} \left|\delta T^{\ell+1}-\delta T^{\ell}\right| \le \text{TOLT} ,$$

where ℓ is iteration number. We have used tolerances of TOLP = 0.05 psi and TOLT = 0.02°F, with a resulting requirement of two to three iterations per time step.

A computational difficulty in the method of solution described above stems from the fact that the method is basically the IMPES (implicit pressure-explicit saturation) procedure commonly applied in black oil simulation.[23-25] This IMPES method suffers from three conditional stability constraints that limit the tolerable time step. The constraints become magnified in the steamflooding case as a result of the extremely large mobility ratios encountered. The conditional stabilities

arise because of explicit treatment of (1) production well rates, (2) capillary pressures, and (3) transmissibilities. Modifications for the implicit treatment of these variables are described in the following sections.

IMPLICIT PRODUCTION RATES

The production rates are expressed implicitly as

$$q_{m,n+1} = q_{m,n} + q_{m,p}\delta p + q_{m,sw}\delta S_w + q_{m,sg}\delta S_g \quad \ldots\ldots\ldots\ldots\ldots\ldots (26)$$

where $m = w, o, g, H$ for water, oil, gas, and enthalpy, respectively. The subscripts p, sw, sg denote partial derivatives with respect to pressure, water, and gas saturations, respectively. The terms $q_{w,sg}$ and $q_{g,sw}$ are zero. These coefficients of δp, δS_w, δS_g augment the appropriate C_{ij} coefficients in the model Eq. 22. The several options in the production routine require somewhat different derivatives for these partial derivatives. For the sake of brevity, we will present here only the case of a well on deliverability producing from a single layer.

The well productivity index (PI) is specified as the quantity

$$PI = \frac{2\pi kh}{\ln\frac{r_e}{r_w} - \frac{1}{2} + S} \times \frac{.00633}{5.6146} \quad \ldots (27)$$

where k is in md, h is in feet, S is skin factor, and r_e is the equivalent radius of the grid block, $\sqrt{\Delta x \Delta y/\pi}$. The production rate of phase $m(m = w,o,g)$ is

$$q_m = PI \cdot \frac{k_{rm} b_m}{\mu_m}(p - p_{well}) \quad \ldots (28)$$

where p_{well} is the specified bottom-hole flowing well pressure and p is the reservoir grid block pressure calculated in the simulator equations. The terms q_{mp} are obtained from Eq. 28 as

$$q_{mp} = PI \cdot \left(\frac{k_{rm} b_m}{\mu_m}\right)_n \qquad m = w, o, g \quad \ldots (29)$$

The term $q_{g,sg}$ is obtained from Eq. 28 as

$$q_{g,sg} = PI \cdot \frac{b_g}{\mu_g}(p - p_{well})\left(\frac{dk_{rg}}{dS_g}\right)_n \quad \ldots (30)$$

The terms $q_{w,sw}$ and $q_{o,sw}$ are calculated using a logic that preserves the total RB/D water plus oil production rate and the term $q_{o,sg}$ is set to zero.

The total RB/D liquid production rate, from Eq. 28, is

$$q^* = PI\left(\frac{k_{rw}}{\mu_w} + \frac{k_{ro}}{\mu_o}\right)_n (p_{n+1} - p_{well}) \quad \ldots (31)$$

The water rate is then

$$q_w = f_w b_w q^* \quad \ldots (32)$$

where f_w is two-phase fractional flow of water, $1/[1 + (k_{ro}/k_{rw})(\mu_w/\mu_o)]$. The saturation partial derivatives are then computed as

$$q_{w,sw} = b_w q^* \left(\frac{df_w}{dS_w}\right)_{chord} \quad \ldots (33a)$$

$$q_{o,sw} = -b_o q^* \left(\frac{df_w}{dS_w}\right)_{chord} \quad \ldots (33b)$$

where

$$\left(\frac{df_w}{dS_w}\right)_{chord} = \frac{f_{wn+1} - f_{wn}}{S_{wn+1} - S_{wn}} \quad \ldots (34)$$

If this chord slope is not used, computed water cut or water/oil ratio can deviate considerably from that given by computed water saturation at the end of the time step and the water/oil relative permeability table. A factor of 0.5 can be used on the right-hand side of Eq. 34 to obtain a water cut equal to the average of the cuts at S_{wn} and S_{wn+1}.

IMPLICIT TRANSMISSIBILITIES AND CAPILLARY PRESSURE

In the normal, explicit IMPES procedure, Eq. 1 is solved directly for δS_w after the pressure equation, Eq. 25 is solved. We will denote the change in water saturation thus obtained by δS_w. MacDonald and Coats[26] suggested a modified IMPES method in which saturations are calculated from the respective flow equations, with transmissibilities expressed implicitly. Using MacDonald's extension, we calculate a somewhat different water saturation change, δS_w, from Eq. 1 written with transmissibility and capillary pressure expressed implicitly:

$$-q_c + \frac{V}{\Delta t} S_{wn}\delta(\phi b_w) + \frac{V}{\Delta t}(\phi b_w)_{n+1}\hat{\delta S}_w = \Delta\left[(T_{wn} + \delta T_w)(\Delta(p_{wn} + \delta p - \delta P_{cwo}) - \gamma_w \Delta Z)\right] - q_{wn} - q_{wp}\delta p - q_{w,sw}\hat{\delta S}_w \quad \ldots (35)$$

Subtraction of Eq. 1, expressed explicitly, from Eq. 35 gives

$$\left(\frac{V}{\Delta t}(\phi b_w)_{n+1} + q_{w,sw}\right)\delta\tilde{S}_w$$

$$= \left(\frac{V}{\Delta t}(\phi b_w)_{n+1} + q_{w,sw}\right)\delta S_w$$

$$+ \Delta(\delta T_w \Delta(p_{wn} + \delta p)) - \Delta(T_{wn}\Delta\delta P_{cwo}) \quad . \quad . \quad (36)$$

where we have dropped the nonlinear term involving the product $\delta T_w \cdot \delta P_{cwo}$. The terms δp and δS_w are known. The changes in transmissibility and capillary pressure are represented in terms of water saturation changes $\delta\tilde{S}_w$. Performing some algebraic manipulation, then, we find that Eq. 36 is simply a parabolic-type difference equation in $\delta\tilde{S}_w$, similar in form to the pressure equation, Eq. 25. Thus, Eq. 36 is easily solved by iterative or direct techniques for $\delta\tilde{S}_w$ over the grid.

A similar treatment of the gas equation (Eq. 2) allows calculation of gas saturation using implicit transmissibility and capillary pressure. However, we are currently calculating δS_g explicitly from Eq. 2. One of several reasons for this choice is a difficulty in implicit treatment posed by large steam flows into blocks where steam is not yet present.

The improved stability given by the implicit Eq. 36 depends significantly upon the method of evaluating the terms δT_w and δP_{cwo}. The term $\delta T_w \Delta(p_{wn} + \delta p) - T_{wn}\Delta\delta P_{cwo}$ in Eq. 36 is the increment in water flow rate between two blocks due to implicit rather than explicit treatment of transmissibility and capillary pressure. There are several different ways to express this implicit increment of flow in terms of water saturation changes $\delta\tilde{S}_w$. The simplest and most stable we have found is

$$\delta T_w = T'_w \delta\tilde{S}_w \quad , \quad . \quad . \quad . \quad . \quad . \quad . \quad . \quad . \quad . \quad . \quad . \quad (37a)$$

$$\delta P_{cwo} = P'_{cwo}\delta\tilde{S}_w \quad , \quad . \quad . \quad . \quad . \quad . \quad . \quad . \quad . \quad . \quad . \quad . \quad (37b)$$

where the product in Eq. 37a is taken at the upstream block and primed quantities are derivatives with respect to S_w evaluated from the tables at S_{wn}. However, this method combined with explicit calculation of δS_g can cause oil saturation to decline below residual. This problem can be avoided by expressing the implicit increment of water flow as $b_w(Q_o + Q_w)f'_w\delta\tilde{S}_w$, where Q is interblock flow rate in RB/D and the total $Q_o + Q_w$ is held fixed at the value determined by the pressure equation, using explicit transmissibilities and explicit capillary pressure. The term f_w is water fractional flow for the oil-water interblock flow stream. f_w can be derived as $f_1(S_w) - f_2(S_w)[(\gamma_w - \gamma_o)\Delta Z - \Delta P_{cwo}]$, where f_1 and f_2 are simple functions of upstream water and oil mobilities. The term f'_w is the derivative or chord slope of this fractional flow with respect to water saturation.

The second approach prevents oil saturations less than residual, but provides less stability than the first. Except for the saturation end-point overshoot, which is only occasionally a problem, the two approaches give essentially the same results in terms of saturation distributions, WOR vs time, etc.

Incremental material balance for water is unaffected by this implicit treatment. An error is introduced in oil incremental material balance that is proportional to the change in water and oil formation volume factors from one block to the next. We have found this error to be negligible, ranging from 0.01 to 0.1 percent of cumulative oil produced at any stage of production.

EFFECT OF GRID ORIENTATION

In simulating five-spot steamflooding, we have found that grid orientation has a great effect on steam breakthrough times. Fig. 1 shows two types of grids representing a five-spot well pattern. Following Todd *et al.*,[27] we refer to these grids as parallel and diagonal grids. The parallel grid results in a far more pronounced steam finger progressing along the injector-producer diagonal. The diagonal grid results in near-radial growth of the steam front with cusping or fingering occurring only as the front approaches the producer.

Steam breakthrough times calculated using the two grids can differ by a factor of more than three. Fig. 2 compares the steam front shapes calculated using the two grids with Relative Permeability Set 1 of Table 2 and Viscosity Curve 1 of Table 3. The initial, mobile water saturation was 0.18.

We have been unable to determine which of the two grids yields the correct result. Todd showed

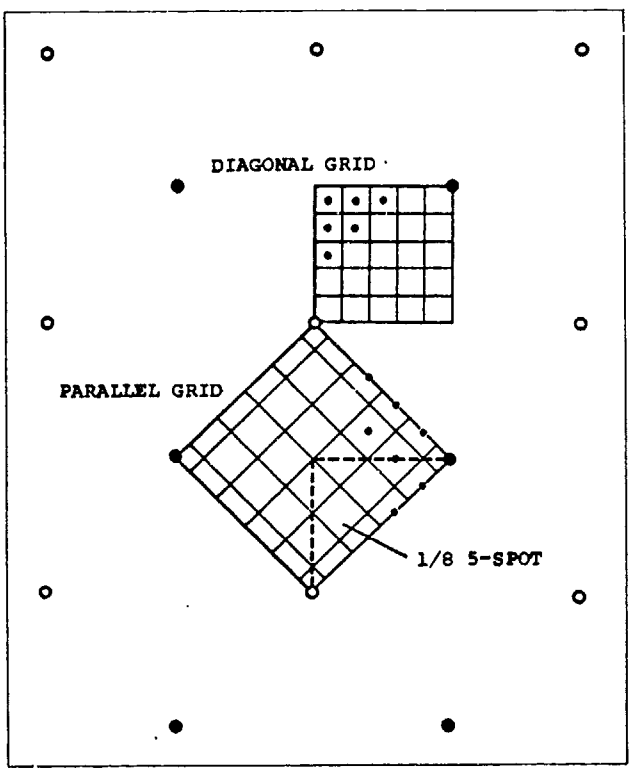

FIG. 1 — PARALLEL AND DIAGONAL GRIDS FOR FIVE-SPOT PATTERN.

that the diagonal grid gave more accurate results in waterflood calculations up to adverse mobility ratio of 10. In theory, we would increase definition of both grids until a single unique answer was obtained and then we would know which grid result is more accurate at coarser definitions. We ran two-dimensional areal simulations of 1/4 five-spots with grid definitions ranging up to 16 × 16 for the diagonal grid and 22 × 22 for the parallel grid. Each grid seemingly converged to an unchanging result at definitions well short of these upper limits. However, the results were completely different for the two grids as shown in Fig. 2. We seemingly have convergence upon different flood performances — at least in relation to frontal shape.

An intuitive approach to this question can easily end in confusion. The nominal mobility ratio of the steamflood, considering 2,400-cp cold oil ahead of the front and 0.01-cp steam behind the front, is on the order of 100,000. This would lead to an intuitive favoring of the parallel grid result in Fig. 2. However, Baker[15] points out that because of condensation, use of kinematic viscosity might give a better indication of effective mobility ratio. This would reduce the ratio to about 500, using a specific volume ratio of 200 between steam and oil. In addition, we are dealing with two fronts in cases where oil banks form. The steam front occurs at the trailing edge of the oil bank, with a near-irreducible water saturation immediately ahead. Mobility ratio at this front is highly unfavorable. Another front occurs at the leading edge of the oil bank. Water saturation is nearly irreducible ahead of this second front. Mobility ratio at this front is highly *favorable*. We must also consider the fact that the disparity in steam front shapes calculated using the two grids persists long after the leading edge of the oil bank has been swept from the reservoir. Finally, we might question the use of oil viscosity or mobility at all in calculating mobility ratios, since most of the total mobility in the oil bank ahead of the steam front stems from the near-irreducible water saturation rather than from the oil mobility.

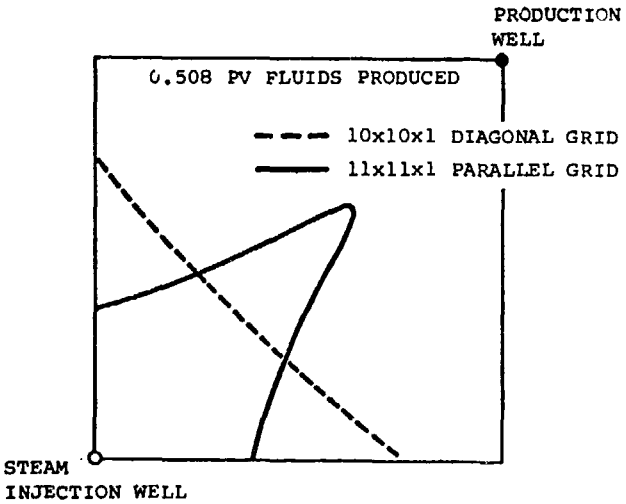

FIG. 2 — COMPARISON OF 20 PERCENT STEAM SATURATION CONTOURS CALCULATED USING DIAGONAL ANL PARALLEL GRIDS.

We simulated a laboratory steamflood using both parallel and diagonal grids and obtained more than a threefold difference in steam breakthrough times. The parallel-grid breakthrough time agreed closely with the observed time. In a representative field-scale run, the parallel grid gave steam breakthrough time slightly in excess of the observed 1 year, whereas the diagonal-grid breakthrough time exceeded 3 years. Both these simulations are discussed in more detail below. While these observations are not conclusive, they pose an argument favoring the accuracy of the parallel grid.

The effect of grid type on calculated oil recovery is far less than the effect on breakthrough times. In both two and three dimensions, we have consistently calculated parallel-grid oil recovery curves virtually identical in shape to and only slightly lower than those calculated from the diagonal grid.

MODEL RESULTS

The model has been applied to a number of problems, including hot waterflooding, steam stimulation using a single-well radial-z grid, laboratory experiments, and field-scale steamfloods. In addition, many runs have been made to determine the sensitivity of model results to different types of input data and to controllable field variables such as rate and injection interval. The data used in the applications reported here are given in Tables 1 through 8. Table 1 gives values of physical constants that have minor effects on calculated results. In some applications, values somewhat different from those given in Table 1 were used. Table 2 gives four sets of relative permeability curves, Table 3 gives two curves of oil viscosity vs temperature, and Table 4 shows water and steam viscosities vs temperature. The discussion of each application below gives the particular set of relative permeability and oil viscosity used.

EXPERIMENTAL DATA OF WILLMAN *ET AL.*

Willman *et al.*[3] reported temperature distributions and oil recovery curves for a number of one-dimensional displacements of oil by steam and hot water. Shutler[9] reported additional data for one series of these experimental runs and compared his mathematical model's results with observed data. The 856-md Torpedo sandstone core was 91.4 cm long and 6 in. in diameter; it was wrapped with fiberglass insulation. The oil used was a 25 percent distillable mixture of Primol and Napoleum having a viscosity of 22.5 cp at the initial 80°F temperature.

Shutler determined relative permeability curves and core thermal constants by trial-and-error

TABLE 1 — BASIC DATA

$b_{wi} = 1.0$	$c_r = 3 \times 10^{-6}$
$b_{oi} = 1.0$	$C_{Tw} = 0.00049$
$c_w = 3.1 \times 10^{-6}$	$C_{To} = 0.0004$
$c_o = 5 \times 10^{-6}$	$C_{po} = 0.5$
	$C_{pw} = 1.0$

matching of the observed temperature distributions and the oil recovery curve from a hot waterflood. Those curves were used in our calculations, together with capillary pressure and fluid viscosity curves given by the same author.

We computed effective thermal conductivity for the core as $\Sigma K_i A_i$ divided by the cross-sectional area of the core. The A_i are cross-sectional areas of sandstone, lead, and the steel core-holder wall. We assumed the core holder was 6-in. Schedule 40 steel pipe. The resulting value for K was 162 Btu/°F-ft-day compared with the value of 100 used by Shutler. A similar weighted calculation of ρC_p for the core, including the heat capacities of sand, lead, and steel, gives ρC_p = 53.1 Btu/(°F)-(cu ft sand grain volume). A value of 31 was employed by Shutler.

For the insulation we used K_{ob} = 0.504 Btu/°F-ft-day and $(\rho C_p)_{ob}$ = 0.567 Btu/°F-cu ft bulk volume. These values compare with respective values of 60 and 6 used by Shutler, implying that he lumped some or all of the lead and steel wall into the "overburden" rather than into the core.

The heat-loss calculation in the steam model was performed in radial geometry using annular ring increments. The hot water and steam injection results shown in Figs. 3 through 5 were computed using NX = 18 grid blocks. Injection and production rates were determined by the model using injectivity/productivity indices reflecting the time-varying (computed) end-block mobilities, pressures, and absolute rock conductivities corresponding to the half-block distances separating core end faces and grid points.

Fig. 3 shows that the calculated recovery curve for hot water injection lies slightly above both Shutler's results and the experimental results. In the steam injection case our calculated oil recovery curve lies below Shutler's but, on the average, exhibits the same moderate agreement with experimental results.

Fig. 4 shows that our calculated temperature profile at 0.55 PV produced in the steam injection case is advanced beyond the experimentally measured profile. In the hot water case, our calculated temperature profile at 0.4 PV produced lies slightly under the experimental values. Shutler's calculated profiles are not indicated on Fig. 4

TABLE 2 — WATER-OIL AND GAS-OIL RELATIVE PERMEABILITY DATA

S_w	k_{rw}	k_{row}	P_{cwo}	$S_{wc} + S_o$	k_{rg}	k_{rog}	P_{cgo}
				Set 1			
0.130	0.0000	1.0000		0.200	0.1700	0.000	0.1000
0.191	0.0051	0.9990		0.395	0.1120	0.0294	0.0756
0.250	0.0102	0.7690		0.433	0.1022	0.0461	0.0709
0.294	0.0168	0.7241		0.515	0.0855	0.0883	0.0606
0.357	0.0275	0.6206		0.569	0.0761	0.1172	0.0539
0.414	0.0424	0.5040		0.614	0.0654	0.1433	0.0483
0.490	0.0665	0.3714		0.663	0.0500	0.1764	0.0421
0.557	0.0970	0.3029		0.719	0.0372	0.2170	0.0351
0.630	0.1148	0.1555		0.750	0.0285	0.2255	0.0313
0.673	0.1259	0.0956		0.805	0.0195	0.2919	0.0244
0.719	0.1381	0.0576		0.850	0.0121	0.3373	0.0188
0.789	0.1636	0.0000		0.899	0.0026	0.5169	0.0126
1.000	1.000	0.0000		1.000	0.0000	1.0000	0.0000
				Set 2			
0.270	0.0000	1.0000		0.360	0.1700	0.0000	
0.355	0.0131	0.5852		0.395	0.1120	0.0294	
0.385	0.0194	0.3784		0.433	0.1022	0.0461	
0.406	0.0235	0.2419		0.515	0.0855	0.0883	
0.427	0.0453	0.2255		0.569	0.0761	0.1172	
0.471	0.0813	0.1238		0.614	0.0654	0.1433	
0.506	0.1167	0.0864		0.663	0.0500	0.1764	
0.538	0.1421	0.0560		0.719	0.0372	0.2170	
0.539	0.1912	0.0283		0.750	0.0285	0.2255	
0.608	0.2300	0.0155		0.805	0.0195	0.2919	
0.633	0.2500	0.0050		0.850	0.0121	0.3373	
0.640	0.2700	0.0000		0.950	0.0000	0.7000	
1.000	0.3100	0.0000		1.000	0.0000	1.0000	
				Set 3			
0.180	0.0000	0.9000	8.00	0.2800	0.3000	0.0000	1.0000
0.250	0.0050	0.6000	4.00	0.6400	0.1500	0.4500	0.5000
0.400	0.0300	0.3000	1.60	1.0000	0.0000	0.9000	0.0000
0.600	0.1100	0.1100	0.50				
0.800	0.1800	0.0000	0.18				
1.000	1.0000	0.0000	0.00				
				Set 4			
0.200	0.0000	1.0000		0.290	0.1700	0.0000	
0.250	0.0102	0.7690		0.395	0.1120	0.0294	
0.294	0.0168	0.7241		0.433	0.1022	0.0461	
0.357	0.0275	0.6206		0.515	0.0855	0.0883	
0.414	0.0424	0.5040		0.569	0.0761	0.1172	
0.490	0.0665	0.3714		0.614	0.0654	0.1433	
0.557	0.0970	0.3029		0.663	0.0500	0.1764	
0.630	0.1148	0.1555		0.719	0.0372	0.2170	
0.673	0.1259	0.0956		0.750	0.0285	0.2255	
0.719	0.1381	0.0576		0.805	0.0195	0.2919	
0.789	0.1636	0.0000		0.850	0.0121	0.3373	
				0.899	0.0026	0.5169	
				1.000	0.0000	1.0000	

TABLE 3 — OIL VISCOSITY VS TEMPERATURE

Set 1		Set 2	
T	μ_o	T	μ_o
75	5,780.0	150	650.0
100	1,380.0	200	160.0
150	187.0	250	56.0
200	47.0	300	24.0
250	17.4	400	6.6
300	8.5	600	2.0
350	5.2	700	1.8
500	2.5		

TABLE 4 — SATURATED WATER AND STEAM VISCOSITIES VS TEMPERATURE

T (°F)	μ_w (cp)	μ_{steam} (cp)
60	1.130	0.0100
80	0.875	0.0106
100	0.685	0.0111
120	0.560	0.0116
150	0.430	0.0124
200	0.308	0.0135
250	0.230	0.0146
300	0.182	0.0157
400	0.145	0.0177
600	0.108	0.0215
740		0.0245

TABLE 5 — LABORATORY MODEL DATA

p_i = 70 psi	K_R = 24
T_i = 75°F	$(\rho C_p)_R$ = 38.6
k = 215 darcies	K_{ob} = 168
ϕ = 0.3063	$(\rho C_p)_{ob}$ = 40
S_{wi} (Run 1) = 0.179	ρ_o = 60.1 lb/cu ft
Steam quality = 0.697 at 204.7 psia	

because they agree virtually identically with the experimental data.

The model calculations assumed no heat loss at the outer insulation boundary. The calculated temperatures at this outer boundary in time reached values closer to core temperatures than to ambient temperature. This is largely because the insulation represented only about 3.9 percent of the total core heat capacity. Thus, the experimental steamflood temperature profile in Fig. 4 may reflect heat loss by radiation and convection from the insulation to the air.

TABLE 6 — STEAM DISPLACEMENT–EXPERIMENTAL DATA

	Run Number				
	1	2	3	4	5
Initial S_o	0.821	0.759	0.682	0.647	0.614
Total fluid injection rate, cc/min	73.7	74.6	73.2	71.8	73.0
Steam quality, percent	69.7	70.0	69.5	68.9	69.4
Time (minutes)	Produced Fluids, PV				
10	0.2026	0.2099	0.2127	0.1867	0.2155
20	0.4198	0.4093	0.4111	0.3893	0.4117
30	0.6185	0.6145	0.6159	0.5820	0.6123
40	0.8082	0.8089	0.7960	0.7704	0.7999
50	1.0093	0.9986	0.9971	0.9520	0.9816
60	1.1890	1.1847	1.1601	1.1500	1.1709
70	1.3746	1.3869	1.3608	1.3183	1.3530
80	1.5637	1.5584	1.5363	1.4948	1.5242
90	1.7462	1.7517	1.7106	1.6702	1.7211
100	1.9278	1.9456	1.8897	1.8517	1.9116
Time (minutes)	Oil Recovery, PV				
10	0.0837	0.0636	0.0407	0.0262	0.0284
20	0.1683	0.1346	0.0829	0.0873	0.0773
30	0.2301	0.2006	0.1378	0.1371	0.1232
40	0.2821	0.2494	0.1782	0.1760	0.1600
50	0.3285	0.2899	0.2168	0.2076	0.1887
60	0.3598	0.3241	0.2406	0.2388	0.2148
70	0.3904	0.3572	0.2724	0.2584	0.2382
80	0.4175	0.3778	0.2885	0.2769	0.2555
90	0.4404	0.4007	0.3046	0.2941	0.2742
100	0.4611	0.4205	0.3227	0.3105	0.2858
Time (minutes)	Injection Well Temperature, °F				
10	340	330	326	335	318
20	317	317	324	320	318
30	317	317	318	315	316
40	317	317	320	315	316
50	315	–	–	–	–
60	315	–	–	–	–
70	315	315	317	315	315
80	315	–	–	–	–
90	315	–	–	–	–
100	315	315	316	315	314
Time (minutes)	Production Well Temperature, °F				
10	150	125	168	75	210
20	195	190	210	200	215
30	182	204	250	215	222
40	192	202	252	220	212
50	198	–	–	–	–
60	217	–	–	–	–
70	282	267	263	300	298
80	302	–	–	–	–
90	305	–	–	–	–
100	307	308	307	305	242

TABLE 7 — DATA FOR REPRESENTATIVE FIELD-SCALE PROBLEM

T_i = 90°F	$K_r = K_{ob}$ = 38.4
p_i = 65 psia	$(\rho C_p)_R = (\rho C_p)_{ob}$ = 35
S_{wi} = 0.50	ρ_o = 60.6
k = 4,000 md	
ϕ = 0.38	

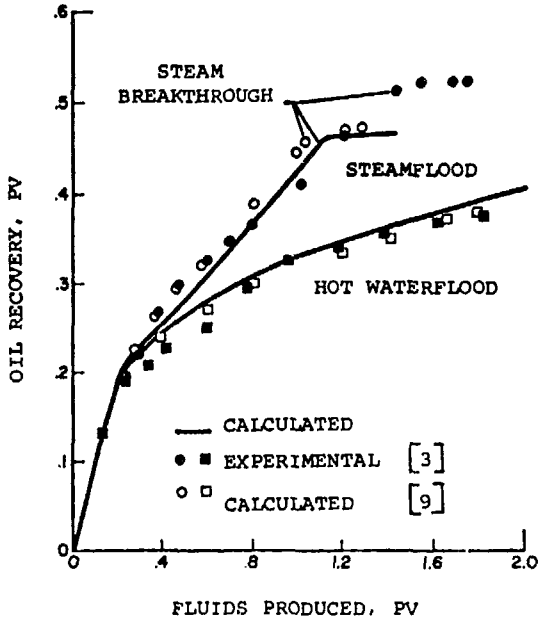

FIG. 3 — COMPARISON OF CALCULATED AND OBSERVED OIL RECOVERY CURVES.

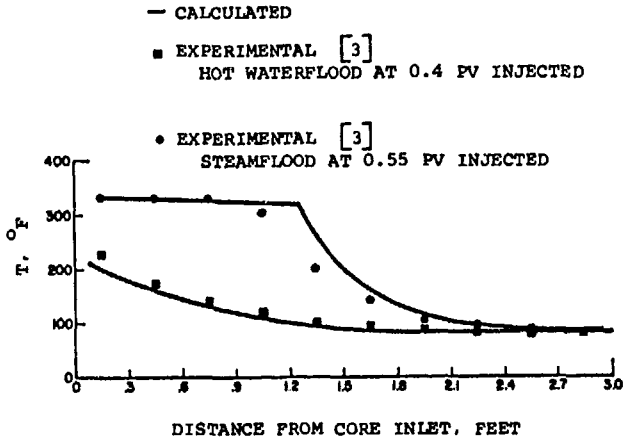

FIG. 4 — COMPARISON OF CALCULATED AND OBSERVED TEMPERATURE PROFILES.

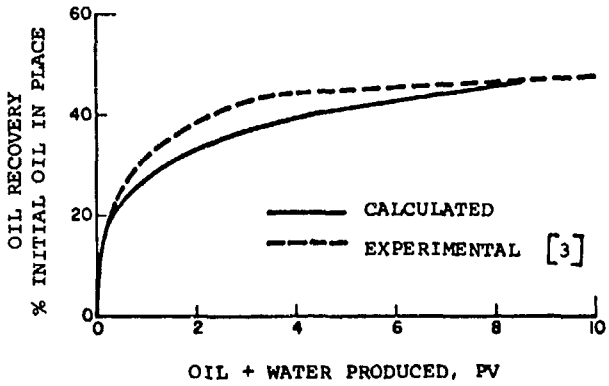

FIG. 5 — COMPARISON OF CALCULATED AND OBSERVED COLD WATERFLOOD RECOVERY.

The sensitivity of the calculated recovery curves shown in Fig. 3 to different types of input data was studied by performing a large number of model runs. We found that relative permeability curves have a significantly greater effect on recovery than any other type of input data. Since no relative permeability curves were measured or reported by Willman *et al.*, they must be determined by trial-and-error matching of recovery curves. This determination is not only tedious and difficult but also questionable from the viewpoint of the whole purpose of model-experiment comparisons. The difficulty is compounded by the introduction of the cold waterflood oil recovery curve shown in Fig. 5. Willman *et al.* report this data for a waterflood using nondistillable oil (Primol) in the same core used for the hot waterfloods and steamfloods. Fig. 5 shows that the water/oil relative permeability curve that Shutler determined results in a significant mismatch of the cold waterflood.

There are undoubtedly sufficient degrees of freedom in the three-phase relative permeability representation to allow matching, with a single representation, of the cold waterflood, hot waterflood, and steamfloods. The above mentioned difficulty stems from the fact that an exhaustive effort may be necessary to find such a representation. The questionable element referred to above is that any representation so found is very probably not unique and claims of model validity based on resulting model-experiment agreement are probably not warranted.

The significance of thermal model-experiment comparisons would be greatly enhanced if relative permeability curves were measured from isothermal floods at each of several temperatures. In addition, initial or preliminary hot water-cold water single-phase experimental runs should be performed to check or validate the model's heat transport calculations.

The calculated oil recovery curves shown in Fig. 3 differ somewhat from Shutler's results. We eliminated a number of possible model or data differences as reasons for the discrepancies. First, in place of Stone's method, we used the three-phase relative permeability representation that Shutler described. Second, as is done in Shutler's model, we altered our model's energy balance to conserve enthalpy in respect to both flow and accumulation terms. Third, we used zero capillary pressure; and fourth, we used Shutler's data for core and overburden thermal constants. None of these changes materially changed our calculated oil recovery curves.

Our steamflood recovery curve agrees significantly more closely with Shutler's if we weight viscosities upstream in the transmissibilities. Also, we used linear interpolation in the relative permeability tables. Shutler might have used curve-fits or more entries not equivalent to our linear interpolation. Very few viscosity-vs-temperature points were provided and our log μ vs log T interpolation may differ from that used by Shutler. The recovery curves are quite sensitive to changes in the μ_o vs T curve.

SHUTLER THREE-DIMENSIONAL EXPERIMENTAL DATA

Shutler[10] gives an oil recovery curve obtained from a laboratory steamflood in a 132-darcy 1/8 confined five-spot. Model dimensions were 10-in. thickness and 3.9-ft distance from injector to producer. We simulated this steamflood using the relative permeability and capillary pressure curves and other data given by Shutler. A diagonal grid with 6 × 6 areal (x-y) definition was used after finding that 8 × 8 and 6 × 6 definitions gave the same results.

Fig. 6 compares the experimental oil recovery curve with curves calculated using 10 × 1 × 1, 6 × 6 × 1 and 6 × 6 × 3 grids. The one- and two-dimensional areal runs gave virtually identical oil recovery curves, indicating the very high areal conformance typically obtained with the diagonal grid. Steam breakthrough occurred at 1.04 PV produced. The three-dimensional calculated curve lies considerably below both the experimental data and the two-dimensional calculated curve. This, together with the three-dimensional calculated steam

TABLE 8 — DATA FOR STEAM STIMULATION EXAMPLE

p_i 1,328 psia	K_R = 32
T_i 120°F	$(\rho C_p)_R$ = 33
h = 100 ft	K_{ob} = 34
Hot water temperature = 330°F	$(\rho C_p)_{ob}$ = 24
r_w = 0.333 ft	ρ_o 56 lb stock tank cu ft
r_e = 940 ft	
Well index (see Eq. 27) = 388	Injection pressure = 1,700 psia
ϕ = 0.32	Production pressure = 800 psia
Well completion = all layers	Pump capacity = 1,400 RB/D

Layer	Horizontal k (md)	Vertical k (md)	S_{wi}
1	1,125	—	0.18
2	1,650	1,375	0.18
3	2,850	2,250	0.188
4	750	1,800	0.206
5	1,725	1,250	0.224

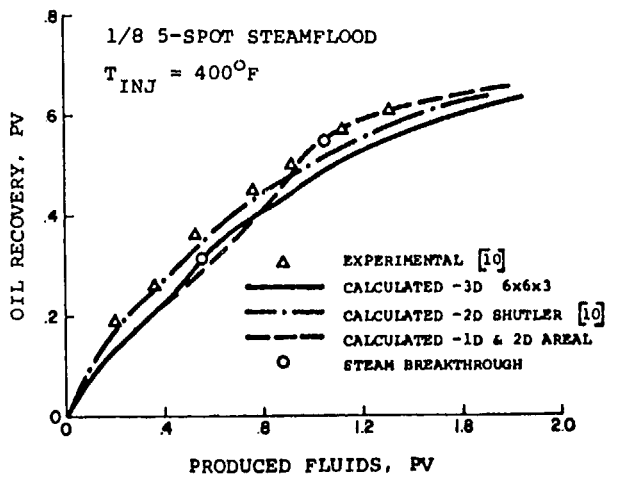

FIG. 6 — COMPARISON OF CALCULATED AND EXPERIMENTAL OIL RECOVERY.

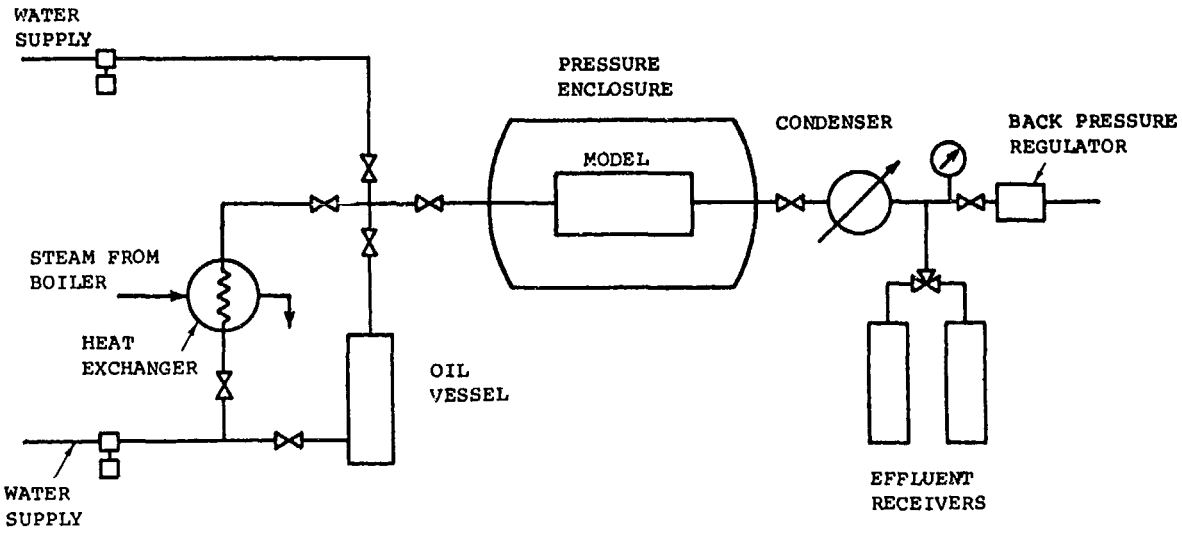

FIG. 7 — SCHEMATIC DIAGRAM OF STEAM DISPLACEMENT EXPERIMENTAL APPARATUS.

breakthrough at 0.55 PV produced, reflects the pronounced steam override. Using a two-dimensional wedge-shaped vertical cross-section, Shutler calculated the recovery curve shown in Fig. 6 that lies between our three-dimensional calculated curve and the experimental data. Using a parallel three-dimensional grid, we calculated an oil recovery curve slightly below that calculated for the diagonal grid, but steam breakthrough occurred at 0.31 PV produced.

Comparison of two- and three-dimensional field-scale five-spot calculations using diagonal grids leads to the same conclusion indicated by the results obtained here. Namely, calculated areal conformance in the confined five-spot is very high, but grid definition in the z-direction is necessary to account for the steam override and low vertical conformance. In unconfined patterns or irregular grid spacing, this behavior dictates three-dimensional modeling.

LABORATORY EXPERIMENTAL DATA

Fig. 7 is a schematic diagram of an experimental apparatus for steam displacement. The physical model consists of a 12- × 12- × 6.4-in. steel box packed with 20-30 mesh Ottawa sand. Injection and production wells at diagonally opposite corners are perforated 1/8-in. tubing extending, respectively, over the lower 3.2 in. and entire 6.4 in. of model thickness. The model dimensions scale to 1/4 of a 2½-acre, 88-ft-thick, confined five-spot.

As shown in Fig. 8, 16 thermocouples are placed as a 4 × 4 square 1/4 in. beneath the top of the model. Another 16 thermocouples are similarly located 1/4 in. above the bottom of the model. In addition, six thermocouples are located midway between top and bottom along two vertical planes perpendicular to the diagonal joining the wells.

The model is contained in a 20-in.-diameter pressure enclosure packed with sand and saturated with water to simulate overburden and underburden formations. The four vertical sides of the model are separated from the surrounding sand by a vacuum space for the purpose of minimizing heat losses from the sides.

The feed system of the model consists of water supply, pumps, a boiler, a heat exchanger, and an oil vessel. Steam generated from the boiler serves as a heating medium in the heat exchanger to

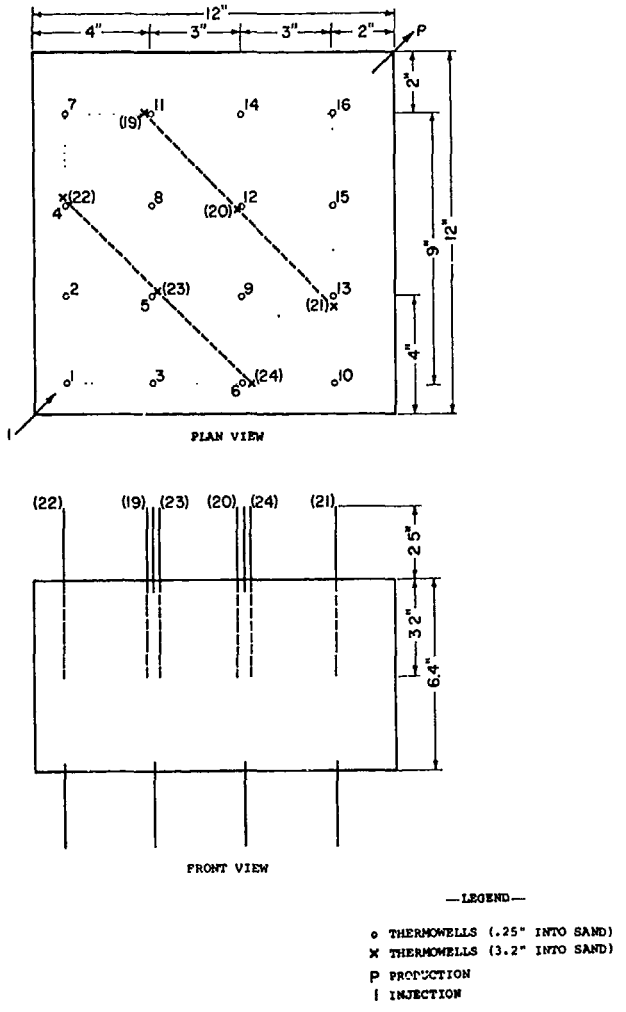

FIG. 8 — PHYSICAL MODEL WITH THERMOCOUPLE LOCATIONS.

generate steam used for steam displacement experiments. This arrangement is necessary to ensure constant injection rates of the steam. Steam from the heat exchanger is combined with water to give a constant rate of injected steam with a constant quality. The effluent train includes a condenser, a backpressure regulator, and effluent receivers where oil and water are separated. A backpressure of 70 psig is normally maintained.

Before each experiment, the model is thoroughly cleaned, dried, and saturated with water. Oil and water are then simultaneously injected in a specified ratio to obtain the desired initial saturations.

The sand in the model has a porosity of 30.63 percent and a permeability of 215 darcies. The experimentally determined relative permeability curves are Set 1 in Table 2. At 75°F, the crude has a density of 60.1 lb/cu ft. Oil viscosity vs temperature is given as Curve 1 in Table 3. Table 5 gives additional data.

Experimental data from five runs representing various initial oil saturations are given in Table 6. Isotherm plots of Run 1 at various times are shown in Fig. 9. These isotherms were obtained by linear interpolation between data points and should be considered to represent approximate positions. The 20 plots included in Fig. 9, taken together, indicate the tendency of steam to migrate upward, causing poor vertical conformance of the steamflood.

We performed preliminary areal and cross-sectional simulator runs to determine the minimum grid definition necessary for adequate representation. These runs indicated sufficient accuracy from a 7 × 7 × 4 parallel-grid representation of 1/8 of a five-spot. Further runs showed that results from this grid were nearly identical with those from a 5 × 3 × 4 grid representing the octant indicated by the dashed lines in Fig. 1. The actual octant grid is 7 × 4 × 4 and the replacement of 7 × 4 × 4 by 5 × 3 × 4 results from including the triangular tips in the adjacent blocks. Computer runs using a diagonal three-dimensional grid of equivalent definition did not show the experimentally observed high temperature finger along the diagonal joining the wells.

Fig. 10 compares calculated and observed isotherms at different flood stages for Run 1. Generally good agreement exists between calculated and observed rates of advance of these isotherms along the vertical plane joining the wells. The early absence and later occurrence of a steam override is evident. Fig. 11 compares calculated and observed isotherms in a vertical plane perpendicular to a line joining the wells. The calculated and observed

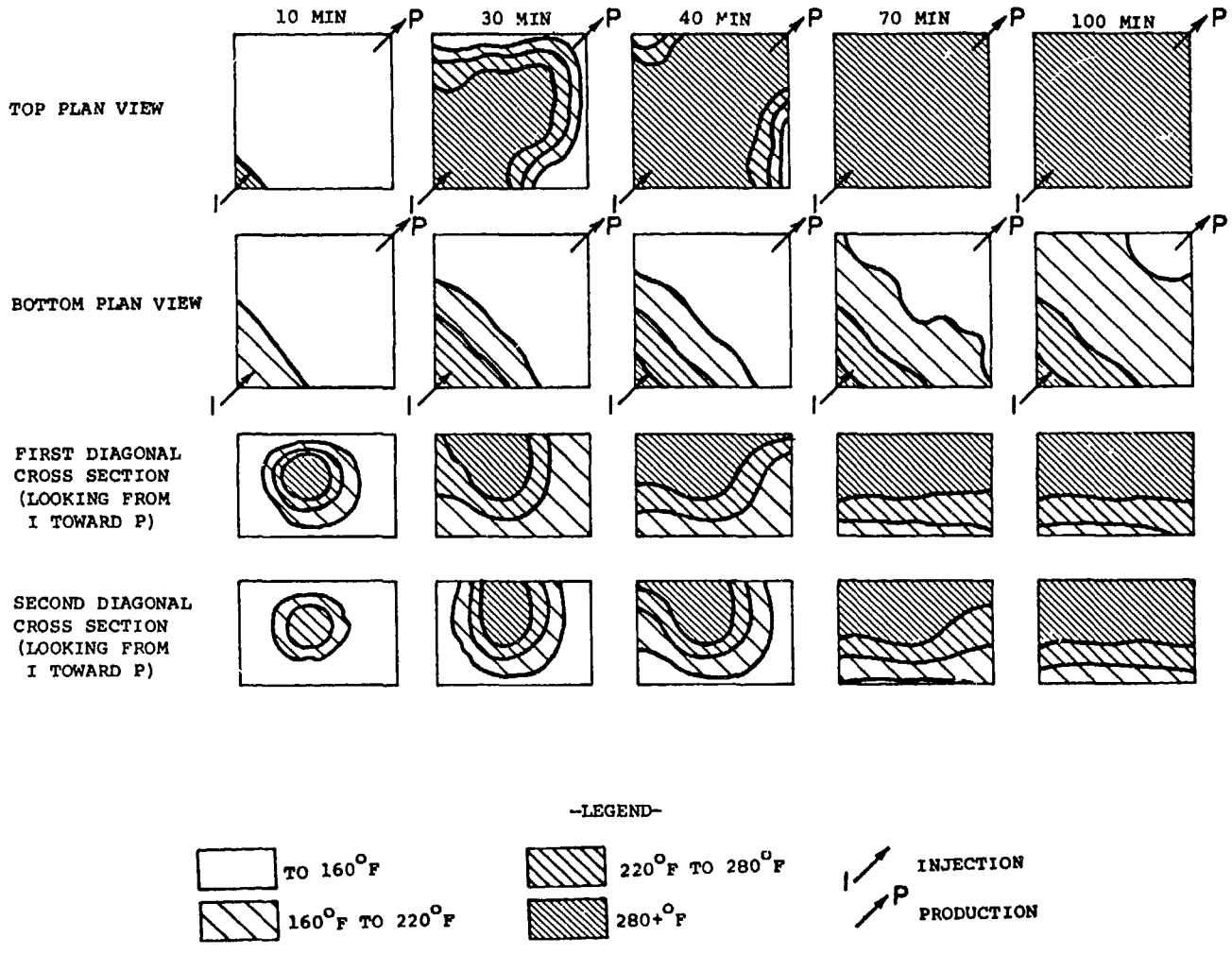

FIG. 9 — EXPERIMENTAL ISOTHERMS, RUN 1.

isotherms are quite different at 30 minutes, largely because of a lack of symmetry in the observed isotherms, reflecting the nonhomogeneity of the physical model.

Fig. 12 shows that the calculated oil recovery curve at first lies beneath and later crosses over the experimental curve. Many factors could contribute to the difference between calculated and observed oil recovery curves. Inhomogeneities in the sand pack or a nonuniform initial saturation distribution can significantly affect the recovery curve. Certain numerical model runs using high permeability streaks gave better agreement with the observed oil recovery curve. Use of modified relative permeability curves also resulted in better agreement. Temperature dependence of relative permeability could account for a major portion of the difference between calculated and observed recovery.

REPRESENTATIVE FIELD-SCALE PROBLEM

A typical field-scale steam displacement pattern was taken to be a 2½-acre five-spot with a net sand thickness of 65 ft. Steam injection rate was 300 to 400 B/D cold water equivalent steam, and breakthrough occurred 6 to 12 months after the start of injection. Fig. 13 shows 6 years of oil production vs time for this typical pattern.

A three-dimensional simulation was performed using the 5 × 3 × 4 parallel grid discussed above. Data for this calculation are given in Table 7. Relative Permeability Set 2 and Viscosity Curve 1 were used. During the first year, we specified a production rate of 720 B/D total fluid and an injection well bottom-hole pressure of 150 psia. Steam was injected into the bottom two layers of the model and production was taken from all four layers. Well indices, defined in Eq. 27, were 20 and 40 for the injector and producer, respectively.

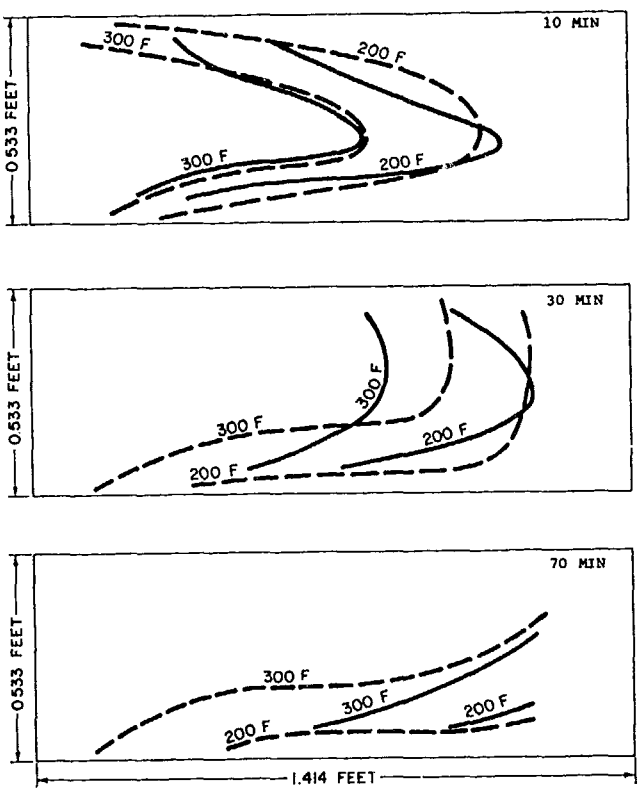

FIG. 10 — CALCULATED AND EXPERIMENTAL ISOTHERMS ALONG CROSS-SECTION FROM INJECTOR TO PRODUCER, RUN 1. SOLID LINES: CALCULATED. DASHED LINES: EXPERIMENTAL.

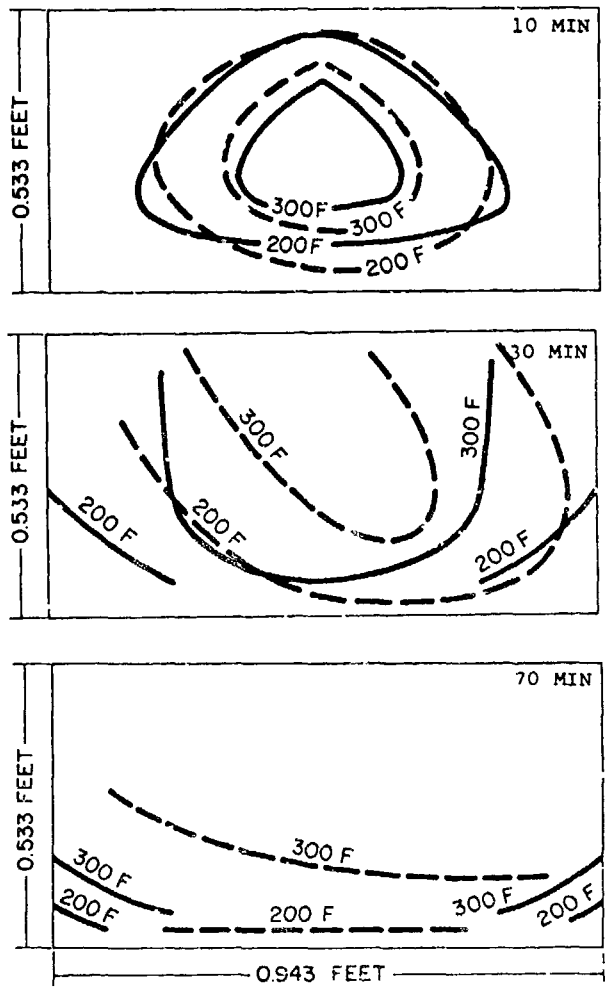

FIG. 11 — CALCULATED AND EXPERIMENTAL ISOTHERMS ALONG FIRST DIAGONAL CROSS-SECTION NORMAL TO LINE JOINING INJECTOR AND PRODUCER, RUN 1. SOLID LINES: CALCULATED. DASHED LINES: EXPERIMENTAL.

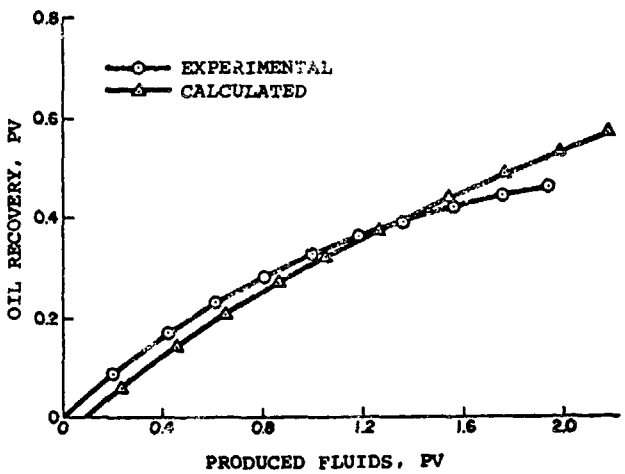

FIG. 12 — COMPARISON OF CALCULATED AND EXPERIMENTAL OIL RECOVERY, RUN 1.

During the remaining 5 years of the run, we specified a steam injection rate of 300 B/D and a production-well bottom-hole pressure of 20 psia. All rates mentioned here are based on a full five-spot.

Calculated results are shown in Figs. 13 through 16. Fig. 13 compares calculated and typical pattern oil production rates. Before production-well response, the calculated rate is much less than the observed rate. The calculated time of production-well response is about 250 days compared with an observed time of about 90 days. After production-well response, the calculated oil rate rises well above the observed rate and then declines into good agreement with field rates over the last 2½ years of the run. The calculated steam breakthrough time of 1 year agrees well with observed times of 6 to 12 months. The calculated average injection rate of 370 B/D during the first year agrees well with observed field injection rates of 300 to 400 B/D.

Figs. 14 and 15 show calculated steam saturation contours in the vertical plane joining the wells and in the top-layer horizontal plane. These contours indicate a pronounced steam override and low areal conformance.

At the economic limit termination of steam injection the model showed that only the upper 75 percent of the reservoir had been displaced of its oil. Fig. 16 shows calculated residual oil saturation contours in the diagonal cross-section from injector to producer. Similar results were obtained in the field from core holes drilled in abandoned steam displacement patterns. The cores showed an average 9 percent residual oil saturation in the upper 60 percent of sand and an average 21 percent oil saturation in the lower 40 percent of sand.

STEAM STIMULATION EXAMPLE

An option in the numerical model allows simulation of single-well performance using the two-dimensional r-z grid commonly used in coning calculations. This option allows simulation of the steam stimulation operation involving cycles of steam injection, soak, and producing periods. The purpose of such model applications is to estimate the effects on oil recovery of (1) injection interval location, (2) injection rates, (3) steam quality, and (4) relative lengths of the injection, soak, and production periods.

The stimulation example presented here uses fluid and reservoir data somewhat altered from those pertinent to an actual well undergoing stimulation. The model r-z grid consisted of eight blocks radially and five blocks vertically. Table 8 gives fluid and rock property data. Relative Permeability Set 3 and Viscosity Curve 2 were used. Injection steam quality was 0.6 at 1,700 psia.

Calculations were performed for three stimulation cycles. In the first cycle, 4 days of hot water injection were followed by 20 days of steam

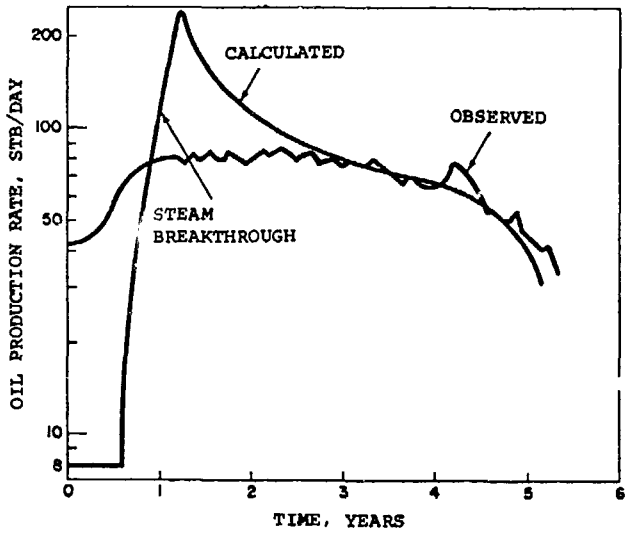

FIG. 13 — CALCULATED AND OBSERVED OIL PRODUCTION RATE, FIELD SCALE FIVE-SPOT STEAMFLOOD.

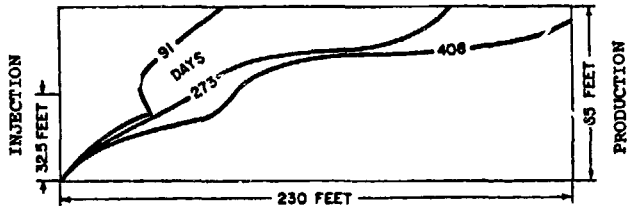

FIG. 14—CALCULATED 30-PERCENT STEAM SATURATION CONTOURS ON DIAGONAL CROSS-SECTION FROM INJECTOR TO PRODUCER; FIELD SCALE FIVE-SPOT STEAMFLOOD.

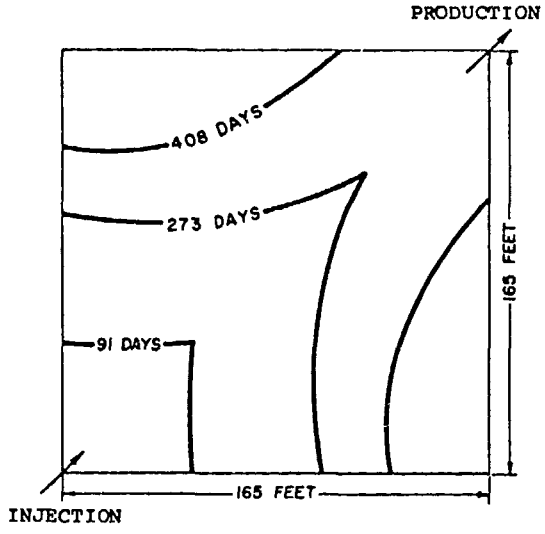

FIG. 15—CALCULATED 30-PERCENT STEAM SATURATION CONTOURS, AREAL VIEW OF LAYER 1; FIELD SCALE FIVE-SPOT STEAMFLOOD.

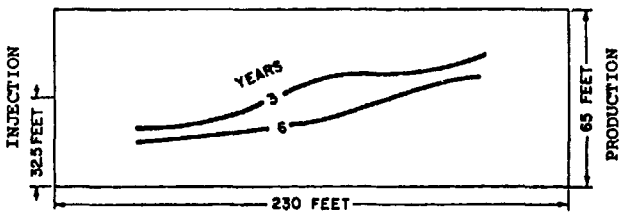

FIG. 16 — CALCULATED 9-PERCENT OIL SATURATION CONTOURS ON DIAGONAL CROSS-SECTION FROM INJECTOR TO PRODUCER; FIELD SCALE FIVE-SPOT STEAMFLOOD.

injection. After a 30-day soak period, the well was produced for 90 days. The second and third cycles were identical except that no hot water was injected.

Fig. 17 shows calculated results. In each cycle the steam injection rate first increases as a result of increased mobility caused by increasing temperature and increasing water and steam saturations near the well. The injection rate then declines as a result of reservoir pressurization. In each subsequent cycle, the steam affects a larger portion of the reservoir and a higher average stimulated oil rate is obtained. Also shown on Fig. 17 is the oil production rate calculated for the case of continuous cold production against the 800-psia bottom-hole flowing pressure. These findings remain to be confirmed by field results.

Tables 9 and 10 show calculated temperatures and saturations at the end of steam injection in Cycles 2 and 3. While the high permeability of Layer 3 combats a steam override, the steam saturations show a partial overriding at the end of the second cycle injection and a more complete override in the third cycle. The exterior radii of Radial Grid Blocks 2, 3, and 4 are 25.1, 45.9, and 84 ft, respectively. The tables show a steam penetration less than 46 ft from the well in the third cycle. In the third cycle, the second layer reaches a temperature of about 200°F 84 ft from the well. All steam condenses during each soak period.

Table 11 compares calculated well performance with and without stimulation. The oil production rates listed are instantaneous rates at the ends of the three cycles — at 144, 278, and 412 days, respectively. The stimulated total oil recovery of 40,340 STB was 55 percent more than the cold production oil recovery. The total steam injection of 51,010 STB with a net total water production (difference between stimulated and cold production) of 41,250 bbl. Contrary to this result, in many field cases the total water recovery is significantly less than the steam injection.

EFFECT OF PRESSURE LEVEL

Our calculations have indicated that steamflood oil recovery increases markedly with decreasing flood pressure level. Primary production from a heavy-oil reservoir generally results in significant pressure decline. A steamflood initiated after a period of depletion can then be conducted at low pressures or at higher pressures ranging up to initial pressure. This leads to the question of whether pressure level has a significant effect on steamflood oil recovery.

The effect of pressure level is somewhat complex because of interactive subeffects. A higher pressure level will tend to increase heat losses and reduce

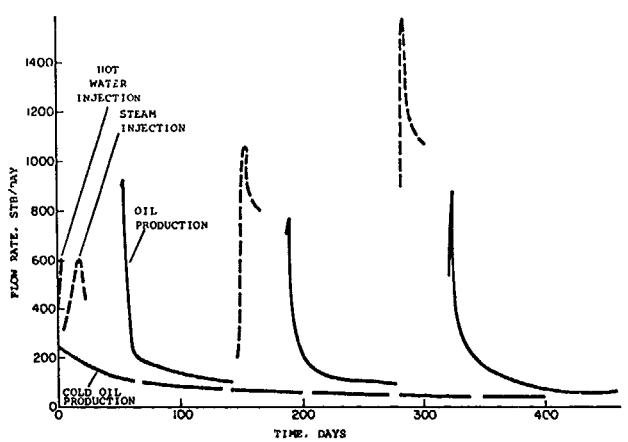

FIG. 17 — STEAM STIMULATION EXAMPLE PRODUCTION-INJECTION RATES.

TABLE 9 — CALCULATED TEMPERATURES AND SATURATIONS FOR STEAM STIMULATION EXAMPLE
(End of Second Cycle Injection – 167 days)

Temperature, °F

	1	2	3	4	5	6	7	8
1	612.5	337.5	160.0	123.5	120.1	120.0	120.0	120.0
2	612.6	612.4	431.7	149.5	120.7	120.0	120.0	120.0
3	612.8	612.8	464.7	163.0	121.4	120.0	120.0	120.0
4	508.9	338.3	180.8	126.9	120.2	120.0	120.0	120.0
5	340.1	203.5	135.9	121.8	120.1	120.0	120.0	120.0

Oil Saturation

	1	2	3	4	5	6	7	8
1	0.4233	0.7155	0.7802	0.8012	0.8125	0.8187	0.8200	0.8200
2	0.2258	0.3867	0.7345	0.7838	0.8050	0.8157	0.8192	0.8199
3	0.1782	0.5123	0.7993	0.8030	0.8040	0.8085	0.8116	0.8133
4	0.6196	0.7418	0.7967	0.7969	0.7937	0.7939	0.7947	0.7957
5	0.7706	0.7869	0.7942	0.7840	0.7768	0.7755	0.7765	0.7773

Gas Saturation

	1	2	3	4	5	6	7	8
1	0.2219	0.0000	0.0000	0.0000	0.0000	0.0000	0.0000	0.0000
2	0.3265	0.2115	0.0000	0.0000	0.0000	0.0000	0.0000	0.0000
3	0.2695	0.0695	0.0000	0.0000	0.0000	0.0000	0.0000	0.0000
4	0.0000	0.0000	0.0000	0.0000	0.0000	0.0000	0.0000	0.0000
5	0.0000	0.0000	0.0000	0.0000	0.0000	0.0000	0.0000	0.0000

TABLE 10 — CALCULATED TEMPERATURES AND SATURATIONS FOR STEAM STIMULATION EXAMPLE
(End of Third Cycle Injection – 301 days)

Temperature, °F

	1	2	3	4	5	6	7	8
1	612.4	612.3	352.3	142.4	120.8	120.0	120.0	120.0
2	612.5	612.4	612.2	244.6	125.7	120.1	120.0	120.0
3	612.8	612.7	529.3	202.2	125.4	120.1	120.0	120.0
4	530.8	395.0	220.8	139.7	121.2	120.0	120.0	120.0
5	364.9	235.5	131.9	126.1	120.5	120.0	120.0	120.0

Oil Saturation

	1	2	3	4	5	6	7	8
1	0.1209	0.2899	0.7035	0.7351	0.8062	0.8164	0.8198	0.8200
2	0.1189	0.2775	0.6901	0.7722	0.7985	0.8123	0.8183	0.8198
3	0.1322	0.4152	0.7764	0.8012	0.8028	0.8066	0.8111	0.8137
4	0.5597	0.7301	0.7932	0.8000	0.7938	0.7939	0.7952	0.7967
5	0.7578	0.7793	0.7922	0.7849	0.7774	0.7759	0.7771	0.7785

Gas Saturation

	1	2	3	4	5	6	7	8
1	0.4016	0.3548	0.0000	0.0000	0.0000	0.0000	0.0000	0.0000
2	0.3543	0.2956	0.0086	0.0000	0.0000	0.0000	0.0000	0.0000
3	0.2938	0.0789	0.0000	0.0000	0.0000	0.0000	0.0000	0.0000
4	0.0000	0.0000	0.0000	0.0000	0.0000	0.0000	0.0000	0.0000
5	0.0000	0.0000	0.0000	0.0000	0.0000	0.0000	0.0000	0.0000

TABLE 11 — SUMMARY OF STEAM STIMULATION RESULTS

	Stimulated Production				Cold Production		
Cycle	Steam Injection (STB)	Oil Production (STB)	Water Production (STB)	Producing Oil Rate (STB/D)	Oil Production (STB)	Water Production (STB)	Producing Oil Rate (STB/D)
1	11,410	14,570	31,680	96	12,900	22,170	66
2	15,640	12,690	28,300	80	7,600	12,960	42
3	23,960	13,080	25,140	58	5,570	8,740	35
Total	51,010	40,340	85,120		26,070	43,870	

oil recovery because of the higher temperature. However, the lower specific volume of steam at the higher pressure will result in a lower rate of steam advance, which tends to give lower heat loss after injection of a given amount of steam. From a displacement point of view, the lower specific volume of steam at higher pressure tends to decrease oil recovery. Finally, the lower oil viscosity at the higher temperature associated with higher pressure tends to result in increased oil recovery at higher pressure.

We simulated a linear steamflood in a reservoir 233 ft long, 116 ft wide, and 65 ft thick. Relative Permeability Set 4 and Viscosity Curve 1 were used. The initial mobile water saturation was 0.30. A high permeability of 40,000 md was used to minimize the pressure gradient in the reservoir. Table 7 gives additional data. We injected steam at a constant rate of 36.1 STB/D in each of two runs with production well pressure held at 100 psia and 500 psia, respectively. At the end of 1,440 days, the total produced fluids were 0.57 PV in the high-pressure flood (530 psia) and 0.69 PV in the low-pressure flood (150 psia). Oil recovery at 1,440 days was 18,878 STB, or 22.5 percent of initial oil in place for the low-pressure flood. The high-pressure flood recovery was only 7,662 STB, or 9.2 percent of initial oil in place. Fig. 18 compares calculated oil recovery with cumulative steam injection for the two floods.

Total injected heat in each run was 16.14×10^9 Btu relative to a base of cold water at 90°F. Calculated heat loss at 1,440 days was 8.14×10^9 Btu in the high-pressure flood and 8.43×10^9 Btu in the low-pressure flood. The high-pressure flood temperature of 473°F considerably exceeded the low-pressure flood temperature of 359°F. In spite of this difference, heat loss was greater in the low-pressure flood. The reason for this greater heat loss is that at 1,440 days, the low-pressure steam front had advanced to more than 40 percent of the reservoir length compared with only 20 percent of length in the high-pressure case. Increasing levels of heat loss tend to reduce the effect of pressure level on recovery.

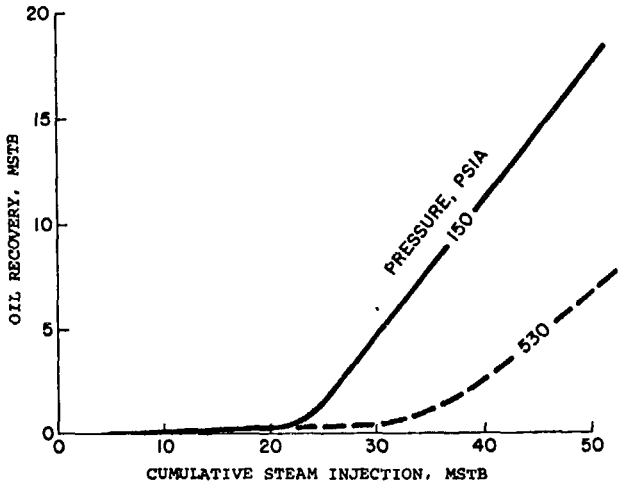

FIG. 18—EFFECT OF PRESSURE LEVEL ON LINEAR STEAMFLOOD OIL RECOVERY.

Steamflood calculations using specified injection and production pressures rather than specified injection rate show an added subeffect of pressure level. This is the increased flood rate achieved at higher pressure for given well indices and injection-production well pressure difference. Calculations for high and low pressure levels using a specified pressure difference have given similar curves of oil recovery vs time. However, even in this case, the ratio of STB oil recovered per STB steam injected is still considerably larger at lower flood pressure.

MODEL RUNNING TIME

One-dimensional runs require about 0.005 seconds per grid block per time step on the CDC 6600. The two- and three-dimensional runs described in this paper required about 0.007 seconds per block-step. A 20-block one-dimensional steamflood, using the data described above for the representative field-scale flood calculation, required 21 CDC 6600 seconds and took 230 time steps. This model performance was unaffected by the occurrence or absence of flow blockage. Shutler[9] reported that his formulation required less than 15 minutes of IBM 360/65 time and 250 time steps for a 20-block one-dimensional steamflood where flow blockage did not occur. This is a time requirement of 0.036 equivalent CDC 6600 seconds per block-step, using a factor of five in computing speeds of the two machines. Abdalla and Coats[11] reported time requirements of 0.008 and 0.01 CDC 6600 seconds per block-step for one- and two-dimensional problems, respectively.

Earlier in the paper we discussed two methods of evaluating terms arising in implicit treatment of transmissibilities. Using the more stable method, the model required 320 CDC 6600 seconds for the three-dimensional 6-year representative field-scale run described above. This computer time rose to 530 seconds when the less stable method was employed. The steam stimulation example required 133 CDC 6600 seconds for the three stimulation cycles.

DISCUSSION AND CONCLUSIONS

A new formulation and method of solution has been presented for three-dimensional modeling of steam injection processes. This formulation allows for simultaneously solving the fluid mass and energy balances and eliminates the need for iterating on the mass transfer (condensation) term. Use of implicit transmissibilities in the model contributes to the stability and efficiency of the calculations. Running time requirements for the model are less than those for previously described formulations.

Laboratory steamflood data are reported for a 1/4 five-spot exhibiting three-dimensional flow effects. These data include temperature distributions and oil recovery vs time and allow checking of assumptions and accuracy of numerical models.

All of our model comparisons with experimental data exhibit calculated oil recovery curves lying below the experimental curves. We performed many model runs with altered data in attempts to reduce the differences between calculated and observed oil recovery. Of all the rock and fluid input data, the water relative permeability curve consistently showed the strongest effect on this disparity. Our tentative conclusion is that temperature dependence of relative permeability must be incorporated in the model to adequately reproduce observed oil recovery. Previous authors,[9-11] to the contrary, concluded that their models, using no such temperature dependence, agreed satisfactorily with experimental data.

We found a pronounced difference in calculated areal conformances of a confined five-spot as calculated using parallel and diagonal grids. As stated previously, we have been unable to determine which, if either, of these grids yields the correct conformance. Possible approaches to this question include comparisons with detailed experimental data, use of variational or higher-order finite-difference schemes in the model, and use of orthogonal, but nonrectangular, grid networks.

Model calculations indicate a strong effect of steamflood pressure level on recovery. In spite of lower oil viscosity at higher pressure levels, recovery is considerably greater at lower flood pressure.

Model calculations for 6- to 10-in.-thick laboratory models and 60-ft-thick field cases show pronounced steam override. This indicates the need for three-dimensional modeling in cases of unconfined patterns or irregular well spacing. For the confined five-spot, a diagonal grid results in such high calculated areal conformance that a two-dimensional wedge-shaped cross-section yields the same results as a full three-dimensional calculation. A parallel grid, however, gives low areal conformance and leads to the necessity of three-dimensional modeling for the confined five-spot.

An example problem indicates that the model formulation can efficiently simulate the single-well, cyclic steam stimulation problem. Comparison of water production in this example with reported production in field cases tends to indicate a need for temperature dependence of water relative permeability.

NOMENCLATURE

b = formation volume factor, STB/RB for oil, mol/RB for water and steam
b_{oi} = oil formation volume factor at T_i, p_i
b_{wi} = water formation volume factor at T_i, p_i
c = compressibility, vol/vol-psi
C_p = specific heat, Btu/lb-°F
C_T = thermal expansion coefficient, vol/vol-°F
f_w = fractional flow of water
H = enthalpy
k = permeability
k_r = relative permeability
K = thermal conductivity, Btu/°F-ft-day
NX, NY, NZ = numbers of grid blocks in reservoir in x, y and z directions, respectively
q_c = rate of steam condensation in grid block
q_H = rate of enthalpy production from grid block $q_w H_w + q_o H_o + q_g H_g$
q_L = rate of heat loss from grid block
q_w = rate of production of water from grid block
p = pressure
p_i = initial reservoir pressure
P_c = capillary pressure
r_w = wellbore radius
S = saturation
S_{wi} = initial water saturation
t = time
Δt = time increment, $t_{n+1} - t_n$
T = temperature
T_c = heat conduction transmissibility, (KA/ℓ)
T_H = enthalpy transmissibility, $T_w H_w + T_o H_o + T_g H_g$
T_i = initial reservoir temperature
T_o, T_g = oil and gas transmissibilities
T_s = temperature of saturated steam
T_w = water transmissibility, $(kA/\ell) b_w k_{rw} / \mu_w$
U = internal energy
V = grid block volume, $\Delta x \cdot \Delta y \cdot \Delta z$
x, y, z = Cartesian coordinates
$\Delta x, \Delta y, \Delta z$ = grid block dimensions
Z = depth measured vertically downward
δ = time difference operator (see Eq. 11)
γ = specific weight, $\rho g/144 g_c$, psi/ft
μ = viscosity, cp
ρ = density, lb/cu ft
ϕ = porosity, fraction

SUBSCRIPTS

g = gas
i = initial condition
i, j, k = grid block indices
n = time level t_n
o = oil
ob = overburden
R or r = rock
w = water

DIFFERENCE OPERATORS

$$\Delta(T_w \Delta p_w) = \Delta_x(T_w \Delta_x p_w) + \Delta_y(T_w \Delta_y p_w) + \Delta_z(T_w \Delta_z p_w)$$

$$\Delta_x(T_w \Lambda_x p_w) = T_{wi+\frac{1}{2},j,k}(p_{wi+1,j,k} - p_{wi,j,k}) - T_{wi-\frac{1}{2},j,k}(p_{wi,j,k} - p_{wi-1,j,k})$$

ACKNOWLEDGMENTS

We express our appreciation to the management of Getty Oil Co. for their permission to publish this paper. We also thank C. W. Shen and T. C. Doerr for the steam displacement laboratory data and E. V. Pollard for the relative permeability measurements.

REFERENCES

1. Lauwerier, H A.: "The Transport of Heat in an Oil Layer Caused by the Injection of Hot Fluid," *Applied Science Research, Sec. A* (1955) Vol. 5, 145.
2. Marx, J. W., and Langenheim, R. H.: "Reservoir Heating by Hot Fluid Injection," *Trans.*, AIME (1959) Vol. 216, 312-315.
3. Willman, B. T., Valleroy, V. V., Runberg, G. W., Cornelius, A. J., and Powers, L. W.: "Laboratory Studies of Oil Recovery by Steam Injection," *J. Pet. Tech.* (July 1961) 681-690; *Trans.*, AIME, Vol. 222.
4. Satter, A., and Parrish, D. R.: "A Two-Dimensional Analysis of Reservoir Heating by Steam Injection," *Soc. Pet. Eng. J.* (June 1971) 185-197; *Trans.*, AIME, Vol. 251.
5. Mandl, G., and Volek, C. W.: "Heat and Mass Transport in Steam-Drive Processes," *Soc. Pet. Eng. J.* (March 1969) 59-79; *Trans.*, AIME, Vol. 246.
6. Gottfried, B. S.: "A Mathematical Model of Thermal Oil Recovery in Linear Systems," *Soc. Pet. Eng. J.* (Sept. 1965) 196-210; *Trans.*, AIME, Vol. 234.
7. Davidson, L. B., Miller, F. G., and Mueller, T. D.: "A Mathematical Model of Reservoir Response During the Cyclic Injection of Steam," *Soc. Pet. Eng. J.* (June 1967) 174-188; *Trans.*, AIME, Vol. 240.
8. Spillette, A. G., and Nielsen, R. L.: "Two-Dimensional Method for Predicting Hot Waterflood Recovery Behavior," *J. Pet. Tech.* (June 1968) 627-638; *Trans.*, AIME, Vol. 243.
9. Shutler, N. D.: "Numerical Three-Phase Simulation of the Linear Steamflood Process," *Soc. Pet. Eng. J.* (June 1969) 232-246; *Trans.*, AIME, Vol. 246.
10. Shutler, N. D.: "Numerical Three-Phase Model of the Two-Dimensional Steamflood Process," *Soc. Pet. Eng. J.* (Dec. 1970) 405-417; *Trans.*, AIME, Vol. 249.
11. Abdalla, A., and Coats, K. H.: "A Three-Phase, Experimental and Numerical Simulation Study of the Steamflood Process," paper SPE 3600 presented at SPE-AIME 46th Annual Fall Meeting, New Orleans, La., Oct. 3-6, 1971.
12. Shutler, N. D., and Boberg, T. C.: "A One-Dimensional Analytical Technique for Predicting Oil Recovery by Steamflooding," *Soc. Pet. Eng. J.* (Dec. 1972) 489-498.
13. Crichlow, H. B.: "Heat Transfer in Hot Fluid Injection in Porous Media," PhD dissertation, Stanford U., Stanford, Calif. (1972).
14. Baker, P. E.: "An Experimental Study of Heat Flow in Steam Floods," *Soc. Pet. Eng. J.* (March 1969) 89-99; *Trans.*, AIME, Vol. 246.
15. Baker, P. E.: "Effect of Pressure and Rate on Steam Zone Development in Steam Flooding," *Soc. Pet. Eng. J.* (Oct. 1973) 274-284; *Trans.*, AIME, Vol. 255.
16. Edmondson, J. A.: "Effect of Temperature on Waterflooding," *J. Cdn. Pet. Tech.* (1965) Vol. 4, 236.
17. Poston, S. W., Ysrael, S., Hossain, A. K. M. S., Montgomery, E. F. III, and Ramey, H. J., Jr.: "The Effect of Temperature on Irreducible Water Saturation and Relative Permeability of Unconsolidated Sands," *Soc. Pet. Eng. J.* (June 1970) 171-180; *Trans.*, AIME, Vol. 249.
18. Davidson, L. B.: "The Effect of Temperature on the Permeability Ratio of Different Fluid Pairs in Two-Phase Systems," *J. Pet. Tech.* (Aug. 1969) 1037-1046; *Trans.*, AIME, Vol. 246.
19. Weinbrandt, R. M., and Ramey, H. J., Jr.: "The Effect of Temperature on Relative Permeability of Consolidated Rocks," paper SPE 4142 presented at SPE-AIME 47th Annual Fall Meeting, San Antonio, Tex., Oct. 8-11, 1972.
20. de Haan, H. J., and van Lookeren, J.: "Early Results of the First Large-Scale Steam Soak Project in the Tia Juana Field, Western Venezuela," *J. Pet. Tech.* (Jan. 1969) 101-110; *Trans.*, AIME, Vol. 246.
21. Stone, H. L.: "Probability Method for Estimating Three-Phase Relative Permeability," *J. Pet. Tech.* (Feb. 1970) 214-218; *Trans.*, AIME, Vol. 249.
22. Price, H. S. and Coats, K. H.: "Direct Methods in Reservoir Simulation," *Soc. Pet. Eng. J.* (June 1974) 295-308; *Trans.*, AIME, Vol. 257.
23. Stone, H. L., and Garder, A. O., Jr.: "Analysis of Gas-Cap or Dissolved-Gas Drive Reservoirs," *Soc. Pet. Eng. J.* (June 1961) 92-104; *Trans.*, AIME, Vol. 222.
24. Sheldon, J. W., Harris, C. D., and Bavly, D.: "A Method for General Reservoir Behavior Simulation on Digital Computers," paper SPE 1521-G presented at SPE-AIME 35th Annual Fall Meeting, Denver, Colo., Oct. 2-5, 1960.
25. Coats, K. H.: "Computer Simulation of Three-Phase Flow in Reservoirs," U. of Texas, Austin (Nov. 1968).
26. MacDonald, R. C., and Coats, K. H.: "Methods for Numerical Simulation of Water and Gas Coning," *Soc. Pet. Eng. J.* (Dec. 1970) 425-436; *Trans.*, AIME, Vol. 249.
27. Todd, M. R., O'Dell, P. M., and Hirasaki, G. J.: "Methods for Increased Accuracy in Numerical Reservoir Simulators," *Soc. Pet. Eng. J.* (Dec. 1972) 515-530; *Trans.*, AIME, Vol. 253.
28. Weinstein, H. G.: "A Semi-Analytic Method for Thermal Coupling of Reservoir and Overburden," *Soc. Pet. Eng. J.* (Oct. 1972) 439-447; *Trans.*, AIME, Vol. 255.
29. Weinstein, H. G.: "Extended Semi-Analytic Method for Increasing and Decreasing Boundary Temperature," *Soc. Pet. Eng. J.* (April 1974) 152-164; *Trans.*, AIME, Vol. 257.
30. *Steam Tables*, Combustion Engineering, Inc., Windsor, Conn. (1970).

APPENDIX

HEAT-LOSS CALCULATION

The top and bottom planes of a three-dimensional grid will lose heat by conduction to adjacent strata as formation temperature rises due to steam or hot-water injection. Discussion here is restricted to the overburden since treatment of the underlying strata is identical. The temperature in the overburden obeys the conduction equation.

$$\vec{\nabla} \cdot (K_{ob} \vec{\nabla} T) = (\rho C_p)_{ob} \frac{\partial T}{\partial t} \quad \ldots\ldots (A\text{-}1)$$

We assume that the overburden acts as a semi-infinite medium vertically. Lateral overburden boundaries

(at reservoir grid boundary) are assumed closed to heat flow. The initial and boundary conditions for Eq. A-1 are thus

$$T(x,y,z,o) = T_i$$

$$T(x,y,o,t) = T_R(x,y,t) \quad z = o, x, y \in R$$

$$T(x,y,\infty,t) = T_i$$

$$\vec{\nabla}T \cdot \vec{n} = o \qquad \text{all } t, x, y, z \in S$$

. . . . . (A-2)

where z is measured upward from the reservoir-overburden plane R; T_i is initial temperature; T_R is the variable reservoir temperature at $z = 0$; S is the overburden lateral surface boundary coinciding in x-y dimensions with the exterior reservoir boundary; and $\vec{n}$ is the normal to S.

We assume uniform or constant K_{ob} and $(\rho C_p)_{ob}$ and negligible effects of heat conduction in the x and y directions. These assumptions reduce the heat-loss equation (Eq. 38) to

$$K_{ob}\frac{\partial^2 T}{\partial z^2} = (\rho C_p)_{ob}\frac{\partial T}{\partial t} \quad . \quad . \quad . \quad . \quad . \quad (A\text{-}3)$$

This equation is represented by the standard central-difference, implicit finite-difference form over a variably spaced grid using small Δz at the reservoir-overburden boundary and increasing Δz away from the boundary. At the end of each time step the finite-difference equation is solved using the known boundary temperature change that occurred over the time step to yield the current temperature distribution in the overburden.

At the beginning of each time step (t_n), then, we we have the finite-difference equivalent of $T(x, y, z, t_n)$. The solution T to the equation is separated into two components, T_1 and T_2. T_1 satisfies Eq. A-3 and the initial and boundary conditions

$$T_1(x,y,o,t) = T(x,y,o,t_n) \qquad t_n < t < t_n + 1$$

$$T_1(x,y,z,t_n) = T(x,y,z,t_n) \quad , \quad . \quad . \quad (A\text{-}4)$$

and T_2 satisfies Eq. A-3 and the conditions

$$T_2(x,y,o,t) = 1 \qquad t_n < t < t_{n+1}$$

$$T_2(x,y,z,t_n) = 0 \quad . \quad . \quad . \quad . \quad . \quad . \quad . \quad . \quad (A\text{-}5)$$

The solution $T(x, y, z, t_{n+1})$ corresponding to a temperature change of δT at the boundary over the $t_n \rightarrow t_{n+1}$ time step is then the sum

$$T(x,y,z,t_{n+1}) = T_1(x,y,z,t_{n+1}) + T_2(x,y,z,t_{n+1})\delta T \quad . \quad . \quad . \quad . \quad (A\text{-}6)$$

From the finite-difference equivalent of T_1, we calculate the rate of heat loss that would occur *during the time step if no* boundary (*reservoir*) temperature change occurred, $q_{L,n}$. The solution T_2 allows calculation of the additional heat-loss rate that will occur if boundary ($k = 1$) temperature increases by δT. Thus, the heat-loss rate for each reservoir grid block in the top plane of the reservoir grid is of the form

$$q_L = q_{Ln} + \alpha \delta T \quad . \quad . \quad . \quad . \quad . \quad . \quad . \quad . \quad . \quad . \quad (A\text{-}7)$$

The one-dimensional finite-difference solution of Eq. A-3 must be performed each time step for each column of overburden — i.e., for each reservoir grid block $(i,j,1)$ $i = 1, NX$, $j = 1, NY$. If $NZ = 1$, then the heat loss calculated for the overburden is simply doubled to account for heat loss to the underlying strata. If $NZ > 1$, this one-dimensional calculation must also be performed for each grid block in the lowest plane (i, j, NZ), $i = 1, NX$, $j = 1, NY$.

Storage requirements for this heat-loss calculation for the three-dimensional case, using six grid blocks to represent the overburden, consist of $5 \cdot NX \cdot NY$ locations for temperature in the overburden and for the underlying strata. The total requirement of $10 \cdot NX \cdot NY$ locations is equivalent to only two full three-dimensional arrays in a problem where $NZ = 5$. Thus the storage requirement is not a serious concern. The computing time requirement for this heat-loss calculation is insignificant — less than 3 percent of total computing time.

The validity of neglecting the x- and y-direction conduction terms was checked by comparing model runs with a simple conduction-convection model. A program was written to solve the implicit finite-difference representation of the conduction-convection heat equation.

$$\frac{\partial}{\partial x}\left(K\frac{\partial T}{\partial x}\right) + \frac{\partial}{\partial z}\left(K\frac{\partial T}{\partial z}\right) - u_w \rho_w C_{pw}\frac{\partial T}{\partial x} = (\phi \rho_w C_{pw} + (1-\phi)\rho_s C_{ps})\frac{\partial T}{\partial t} \quad . \quad . \quad (A\text{-}8)$$

This equation describes heat transport by conduction and convection in a water-saturated two-dimensional porous medium. The program was written to treat either an x-z Cartesian system or an x-r cylindrical system. C_{ps} and ρ_s are specific heat and density, respectively, of solid-sand grains in a core, or of insulation surrounding the core.

This conduction-convection model was used for two purposes. First, fine-grid runs were made to allow checking of the steam model heat-loss calculation. Steam model runs were conducted to simulate hot water injection into a reservoir

initially saturated 100 percent with cold water. Comparisons with the conduction-convection model showed satisfactory agreement between temperature distributions when five or more blocks were used to represent the overburden in the steam model. Accuracy of the conduction-convection model solution was indicated by insensitivity to further grid refinement and by exact heat balances. Explicit treatment of the convection term in Eq. A-8 also results in more accuracy for a given grid than does implicit treatment.

The second application of the conduction-convection model was for checking the assumption regarding x- and y-direction overburden conduction effects. The model has been run for a wide variety of x-z configurations and has consistently shown virtually no effect on reservoir temperatures due to overburden lateral conduction. We found no significant effect of lateral overburden conduction on reservoir temperatures in any flood type of run. The effect of this lateral conduction is detectable in single-well steam stimulation runs where the heated zone remains near the well and heat is continuously lost laterally by conduction through both the reservoir and the overburden. But even in this case, we found a maximum error in reservoir temperatures due to neglect of lateral overburden conduction of several degrees relative to temperature changes of several hundred degrees. The error in reservoir temperature change was on the order of 4 percent or less.

Another option of heat-loss calculation included in the numerical model embodies a simplified version of Weinstein's variational method.[28,29] This version assumes that conduction is negligible in the x and y directions in the overburden. The variational method was applied to two test problems and compared with the superposition method and the finite-difference method using six layers. The superposition method gave the true solution, whereas the other methods provided approximations. In the first test problem, there was assumed a sequence of temperatures on the boundary that contained four temperatures reversals. Although all results were close to one another, the variational method gave results between those from the other two. Another test problem used the temperatures inside the reservoir on a quarter of a five-spot pattern simulated on a 5×5 grid. The variational method was again found to give results closer to those of the superposition method compared with the finite-difference method. The variational method needs five additional arrays, comparable with the finite-difference method using six layers. The computer time requirement of the variational method was also found to be comparable with that of the finite-difference method using six layers.

***